Identification of Store-independent and Store-operated Ca^{2+} Conductances in *Caenorhabditis elegans* Intestinal Epithelial Cells

Ana Y. Estevez,[1] Randolph K. Roberts,[1,4] and Kevin Strange[1,2,3]

[1]Department of Anesthesiology, [2]Department of Molecular Physiology and Biophysics, and [3]Department of Pharmacology, Vanderbilt University Medical Center, Nashville, TN 37232

[4]School of Natural and Health Sciences, Barry University, Miami Shores, FL 33161

ABSTRACT The nematode *Caenorhabditis elegans* offers significant experimental advantages for defining the genetic basis of diverse biological processes. Genetic and physiological analyses have demonstrated that inositol-1,4,5-trisphosphate (IP_3)–dependent Ca^{2+} oscillations in intestinal epithelial cells play a central role in regulating the nematode defecation cycle, an ultradian rhythm with a periodicity of 45–50 s. Patch clamp studies combined with behavioral assays and forward and reverse genetic screening would provide a powerful approach for defining the molecular details of oscillatory Ca^{2+} signaling. However, electrophysiological characterization of the intestinal epithelium has not been possible because of its relative inaccessibility. We developed primary intestinal epithelial cell cultures that circumvent this problem. Intestinal cells express two highly Ca^{2+}-selective, voltage-independent conductances. One conductance, I_{ORCa}, is constitutively active, exhibits strong outward rectification, is 60–70-fold more selective for Ca^{2+} than Na^+, is inhibited by intracellular Mg^{2+} with a $K_{1/2}$ of 692 μM, and is insensitive to Ca^{2+} store depletion. Inhibition of I_{ORCa} with high intracellular Mg^{2+} concentrations revealed the presence of a small amplitude conductance that was activated by passive depletion of intracellular Ca^{2+} stores. Active depletion of Ca^{2+} stores with IP_3 or ionomycin increased the rate of current activation ~8- and ~22-fold compared with passive store depletion. The store-operated conductance, I_{SOC}, exhibits strong inward rectification, and the channel is highly selective for Ca^{2+} over monovalent cations with a divalent cation selectivity sequence of $Ca^{2+} > Ba^{2+} \approx Sr^{2+}$. Reversal potentials for I_{SOC} could not be detected accurately between 0 and +80 mV, suggesting that P_{Ca}/P_{Na} of the channel may exceed 1,000:1. Lanthanum, SKF 96365, and 2-APB inhibit both I_{ORCa} and I_{SOC} reversibly. Our studies provide the first detailed electrophysiological characterization of voltage-independent Ca^{2+} conductances in *C. elegans* and form the foundation for ongoing genetic and molecular studies aimed at identifying the genes that encode the intestinal cell channels, for defining mechanisms of channel regulation and for defining their roles in oscillatory Ca^{2+} signaling.

KEY WORDS: calcium oscillations • biorhythm • calcium channel • inositol-1,4,5-trisphosphate • MIC • CRAC

INTRODUCTION

Fluctuating intracellular Ca^{2+} concentration is a ubiquitous signaling mechanism that controls numerous cellular processes, including gene expression, exocytosis and secretion, motility, cell proliferation, programmed cell death, and differentiation (Berridge et al., 2000). Elevation of cytoplasmic Ca^{2+} levels is brought about by Ca^{2+} release from intracellular stores and by influx across the plasma membrane. In excitable cells, Ca^{2+} influx is mediated to a large extent by voltage- and ligand-gated cation channels. Calcium influx into nonexcitable cells, such as blood cells and endothelial and epithelial cells, occurs primarily via second messenger– and store-operated Ca^{2+} channels (SMOCCs and SOCCs)* (Elliott, 2001; Zitt et al., 2002).

The ER is the principal Ca^{2+} store in nonexcitable cells. Agonist binding to plasma membrane tyrosine kinase– or G protein–coupled receptors activates phospholipase C, leading to the production of inositol 1,4,5-trisphosphate (IP_3). IP_3, in turn, activates IP_3 receptors in the ER membrane, inducing Ca^{2+} release that leads to either a sustained elevation of cytoplasmic Ca^{2+} concentration or Ca^{2+} oscillations (Shuttleworth, 1999; Berridge et al., 2000). Sustained Ca^{2+} elevation is often observed with high agonist concentrations and occurs in a biphasic manner. The first phase involves ER Ca^{2+} release. As the stores are depleted of Ca^{2+}, SOCCs are activated, allowing Ca^{2+} to enter from the extracellular medium (Parekh and Penner, 1997; Taylor and Thorn, 2001). Cytoplasmic Ca^{2+} levels and Ca^{2+} influx remain elevated as long as the stimulus is maintained (Putney and McKay, 1999; Shuttleworth, 1999).

Lower concentrations of agonists typically trigger Ca^{2+} oscillations (Shuttleworth, 1999). The role of plasma membrane Ca^{2+} entry in generating and main-

Address correspondence to Kevin Strange, Vanderbilt University Medical Center, T-4202 Medical Center North, Nashville, TN 37232-2520. Fax: (615) 343-3916; email: kevin.strange@vanderbilt.edu

*Abbreviations used in this paper: ARC, arachidonic acid–regulated Ca^{2+} channel; CRAC, Ca^{2+} release–activated channel; DIC, differential interference contrast; IP_3, inositol-1,4,5-trisphosphate; MagNuM, Mg^{2+}-nucleotide–regulated metal ion; MIC, Mg^{2+}-inhibited cation; SMOCC, second messenger–operated Ca^{2+} channel; SOCC, store-operated Ca^{2+} channel; TRP, transient receptor potential.

J. Gen. Physiol. © The Rockefeller University Press • 0022-1295/2003/08/207/17 $8.00
Volume 122 August 2003 207–223
http://www.jgp.org/cgi/doi/10.1085/jgp.200308804

taining the oscillations is unclear (Shuttleworth, 1999). Calcium oscillations in some cell types continue for long periods in the absence of extracellular Ca^{2+} (Lechleiter and Clapham, 1992). In contrast, oscillatory Ca^{2+} signals in other cell types are strictly dependent on Ca^{2+} influx (Torihashi et al., 2002; Wu et al., 2002).

The molecular identity of both SOCCs and SMOCCs, the mechanisms by which they are regulated, and their precise functional roles in local and global Ca^{2+} signaling are unclear. Genetic model organisms provide a number of powerful experimental advantages for defining the genes and genetic pathways involved in biological processes such as Ca^{2+} signaling. The nematode *Caenorhabditis elegans* is a particularly attractive model system for such studies (Barr, 2003; Strange, 2003). *C. elegans* has a short life cycle, is genetically tractable, and has a fully sequenced and well-annotated genome. It is also relatively easy and economical to manipulate and hence characterize gene function in this organism.

C. elegans exhibits a number of relatively simple stereotyped behaviors that have formed the bases for powerful forward genetic screens. The defecation cycle is one such behavior. Defecation is an ultradian rhythm that occurs once every 45–50 s when nematodes are feeding and is mediated by sequential contraction of the posterior body wall muscles, anterior body wall muscles, and enteric muscles (Iwasaki and Thomas, 1997). Loss-of-function mutations in the IP_3 receptor gene *itr-1* slow or eliminate the defecation cycle, whereas overexpression of the gene increases the rate of defecation (Dal Santo et al., 1999). Oscillatory changes in intestinal epithelial cell Ca^{2+} levels track the defecation cycle, with Ca^{2+} levels peaking just before the initiation of posterior body wall muscle contraction. Calcium oscillations are slowed or absent in animals with loss-of-function mutations in *itr-1* (Dal Santo et al., 1999). Dal Santo et al. (1999) have suggested that IP_3-dependent Ca^{2+} signals may control the secretion of a factor from the intestinal epithelium that regulates contraction of surrounding body wall muscles.

The ability to combine physiological tools, such as patch clamp analysis and Ca^{2+} imaging, with behavioral assays and forward and reverse genetic screening would provide a powerful approach for defining the molecular details of intestinal cell IP_3-dependent Ca^{2+} signaling. However, electrophysiological characterization of somatic cells in *C. elegans* is difficult due to the small size of the animal and the presence of a tough, pressurized cuticle that limits access. To circumvent this problem, we recently developed methods that allow the primary culture and terminal differentiation of nematode embryo cells (Christensen et al., 2002).

We report here the electrophysiological characterization of cultured *C. elegans* intestinal epithelial cells. Intestinal cells express two highly Ca^{2+}-selective whole-cell cation conductances. One conductance is insensitive to store depletion, shows strong outward rectification, and is inhibited by intracellular Mg^{2+}. Intracellular Ca^{2+} store depletion activates an inwardly rectifying SOCC current. These studies provide the first detailed electrophysiological characterization of voltage-independent Ca^{2+}-selective cation conductances in *C. elegans* and form the foundation for ongoing genetic and molecular studies aimed at identifying the genes that encode the channels, for defining mechanisms of channel regulation and for defining their roles in oscillatory Ca^{2+} signaling.

MATERIALS AND METHODS

C. elegans Strains

All strains were derived from the wild-type N2 line and maintained at 20–25°C using standard methods (Brenner, 1974). The *elt-2*–GFP strains used in these studies were JR1838 (wIs84) and JM63 (caIs13). GFP strains contain integrated transgenes.

C. elegans Embryonic Cell Culture

Embryonic cells were prepared by treating synchronized adult nematodes with an alkaline hypochlorite solution (0.5 M NaOH and 1% NaOCl) for 5 min (Lewis and Fleming, 1995). Eggs released by this treatment were pelleted by centrifugation and then washed three times with egg buffer containing 118 mM NaCl, 48 mM KCl, 2 mM $CaCl_2$, 2 mM $MgCl_2$, and 25 mM HEPES (pH 7.3, 345 mOsm) (Edgar, 1995). Adult carcasses were separated from washed eggs by density centrifugation in 30% sucrose. The egg layer was removed by pipette and washed one time with egg buffer and then pelleted. Eggshells were removed by resuspending pelleted eggs in egg buffer containing 1–2.5 U/ml of chitinase for 45–90 min at room temperature. After digestion of the eggshell, the suspension was gently pipetted up and down several times to dissociate the cells. Cells were washed two times with L-15 cell culture medium (Life Technologies) containing 10% FBS (Hyclone), 50 U/ml penicillin, and 50 μg/ml streptomycin and adjusted to 345 mOsm with sucrose.

Dissociated embryo cells were filtered through a sterile 5-μm Durapore syringe filter (Millipore) to remove undissociated embryos and newly hatched larvae. Filtered cells were plated on 12-mm-diameter glass coverslips coated with 0.5 mg/ml peanut lectin agglutinin. Cultures were maintained at 24°C in a humidified incubator in L-15 cell culture medium.

Patch Clamp Recordings

Coverslips with cultured embryo cells were placed in the bottom of a bath chamber (model R-26G; Warner Instrument Corp.) that was mounted onto the stage of a Nikon TE300 inverted microscope. Cells were visualized by fluorescence and video-enhanced differential interference contrast (DIC) microscopy.

Patch electrodes were pulled from soft glass capillary tubes (PG10165-4; World Precision Instruments) that had been silanized with dimethyl-dichloro silane. The standard pipette solution for whole-cell recording from intestinal cells contained (mM) 147 sodium gluconate (NaGluconate), 0.6 $CaCl_2$, 1 $MgCl_2$, 10 EGTA or 10 BAPTA, 10 HEPES, 2 Na_2ATP, 0.5 Na_2GTP, pH 7.2 (adjusted with CsOH), 325 mOsm. The standard bath solution contained (mM) 145 NaCl, 1 $CaCl_2$, 5 $MgCl_2$, 10 HEPES, 20 Glucose, pH 7.2

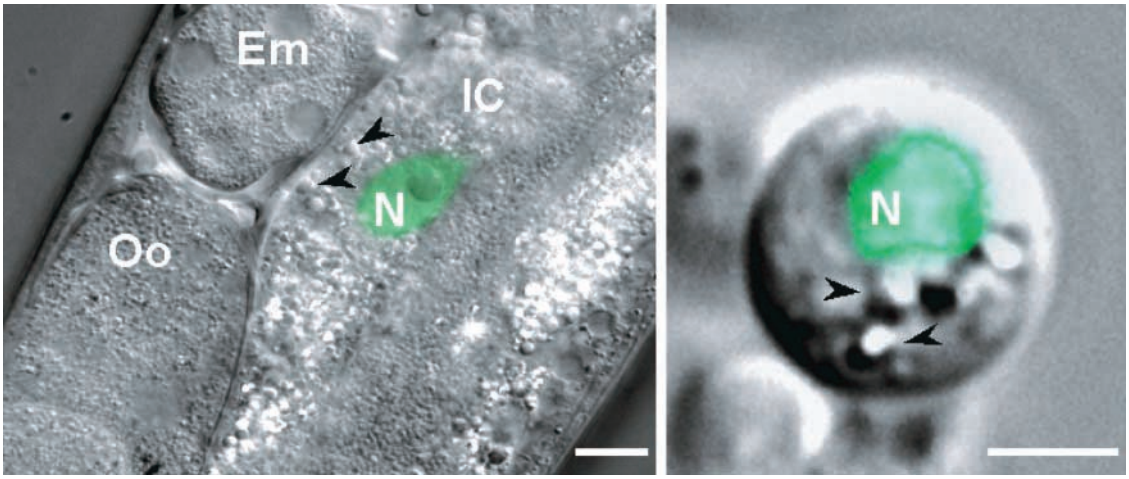

FIGURE 1. Expression of *elt-2*–GFP reporter in *C. elegans* intestinal cells. Images are overlays of DIC and fluorescence micrographs of a transgenic worm (left) and cultured intestinal cell (right) expressing *elt-2*–GFP in the cell nucleus. GFP fluorescence is shown in green. Bars: (left) 10 μm; (right) 2.5 μm. Em, developing embryo in uterus; Oo, oocyte in proximal gonad; IC, intestinal cell; N, intestinal cell nucleus. Arrowheads denote refractile granules that are most likely intracellular storage granules.

(adjusted with NaOH). Osmolality was adjusted to 340–345 mOsm with sucrose. Free Ca^{2+} and free Mg^{2+} levels in the various solutions used were calculated using MaxChelator software WINMAXC v.2.1 (www.stanford.edu/~cpatton/maxc.html).

Whole-cell currents were recorded using an Axopatch 200B (Axon Instruments, Inc.) patch clamp amplifier. Command voltage generation, data digitization, and data analysis were performed on a 1.6-GHz Pentium computer (Dimension 4400; Dell Computer Corp.) using a Digidata 1322A AD/DA interface with pClamp 8.2 and Clampfit 8.2 software (Axon Instruments, Inc.). Currents were filtered at 5 kHz and digitized at 20–40 kHz. Electrical connections to the amplifier were made using Ag/AgCl wires and 3-M KCl/agar bridges.

Ion substitution studies were performed by replacement of bath Na^+ with various test cations. For all ion substitution experiments, changes in liquid junction potentials were measured directly using a free-flowing 3-M KCl electrode. Reversal potentials were corrected for these changes. Relative permeabilities were calculated using the following equations derived from the Goldman-Hodgkin-Katz equation (Lewis, 1979; Hille, 2001):

$$P_X/P_{Na} = \{[X^+]_o/[Na^+]_o\}\exp^{\Delta Erev\ F/RT} \quad (1)$$

$$P_{Ca}/P_{Na} = \{[Na^+]_o/4[Ca^{2+}]_o\}\{\exp^{\Delta Erev\ F/RT}\}\{1+\exp^{ErevCa\ F/RT}\}, \quad (2)$$

where $[X^+]_o$ is the extracellular concentration of the monovalent substitute cation; $[Na^+]_o$ is the extracellular Na^+ concentration; $[Ca^{2+}]_o$ is the extracellular Ca^{2+} concentration; ΔE_{rev} is the change in reversal potential; and F, R, and T have their usual meanings. In studies of the intestinal cell store-operated current, we defined leak current as the current observed immediately after obtaining whole-cell access. This leak current was subtracted from all subsequent current records obtained in the cell.

Chemicals

Thapsigargin, ionomycin, and BAPTA were purchased from Molecular Probes. IP_3 and 2-APB were purchased from Calbiochem. All other chemicals were obtained from Sigma-Aldrich.

Statistical Analyses

Data are presented as means ± SEM. Statistical significance was determined using a two-tailed *t* test or ANOVA followed by a Bonferroni multiple comparisons test. P values of <0.05 were taken to indicate statistical significance.

RESULTS

Identification of C. elegans Intestinal Epithelial Cells in Primary Culture

As described previously, isolated *C. elegans* embryo cells undergo terminal differentiation when cultured in vitro (Christensen et al., 2002). Culturing embryo cells from worm strains expressing cell-specific GFP reporters allows identification of differentiated cell types. ELT-2 is a GATA transcription factor expressed exclusively in intestinal cells and is required for intestinal morphogenesis beginning at the 44–46-cell stage of embryonic development (Fukushige et al., 1999). Primary cell cultures were prepared from worm strains expressing an *elt-2*–GFP transcriptional fusion construct (worm strains provided by J. Rothman [University of California, Santa Barbara, CA] and J. McGhee [University of Calgary, Calgary, Alberta, Canada]). Fig. 1 shows combined DIC and fluorescence micrographs of a transgenic worm expressing *elt-2*–GFP and an intestinal epithelial cell cultured from *elt-2*–GFP-expressing worms.

Our previous studies have shown that various muscle and neuronal cell types in primary culture are present at a frequency remarkably close to that observed in a newly hatched L1 larva (Christensen et al., 2002). An L1 larva is comprised of 558 cells of which 20, or 3.6%, are intestinal cells. Intestinal cells represented 4.1 ± 0.1% ($n = 3$) of the total cells in culture. *elt-2*–GFP expression

was concentrated in the nuclei of cultured intestinal cells (Fig. 1, right), similar to that observed in vivo (Fig. 1, left). In addition, the cytoplasm of the cultured cells contained numerous refractile granules (Fig. 1, right, arrowheads) that were also highly autofluorescent (unpublished data). These most likely represent storage granules, which are a prominent characteristic of intestinal cells in the intact worm (Kostich et al., 2000; Fig. 1, left).

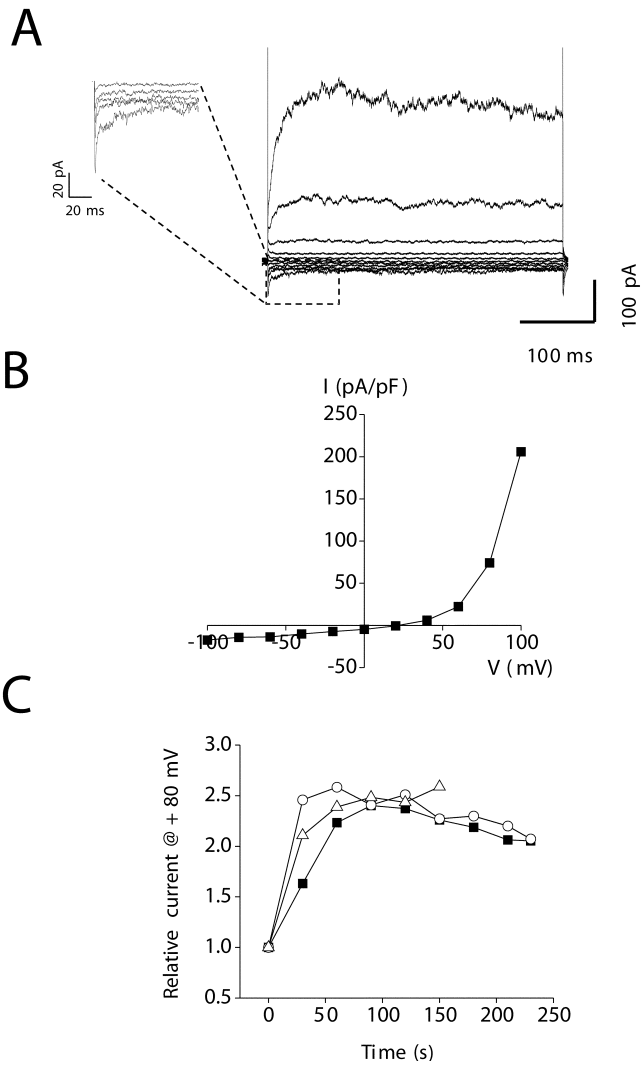

FIGURE 2. Characteristics of outwardly rectifying intestinal cell whole-cell current. (A) Whole-cell currents recorded from a cultured intestinal cell using standard bath (145 mM NaCl) and pipette (147 mM NaGluconate) solutions. Currents were elicited by stepping membrane voltage from −100 to +100 mV in 20-mV steps from a holding potential of 0 mV. Voltage steps were 400 ms long. Inset shows inactivation behavior observed at strongly hyperpolarized voltages. (B) Steady-state I–V relationship for the whole-cell currents shown in A. (C) Whole-cell current activation observed after membrane rupture. Current recordings from three intestinal cells are shown. Values shown are relative to those observed at time 0, which is defined as the time at which whole-cell access was obtained. Whole-cell current typically increased two- to threefold within 1–3 min after membrane rupture and then stabilized.

Intestinal Cells Express an Outwardly Rectifying Cation Current

Cultured intestinal cells were patch clamped readily in the whole-cell mode. An outwardly rectifying whole-cell current (Fig. 2, A and B) was observed when cells were bathed and dialyzed with control bath (145 mM NaCl) and pipette (147 mM NaGluconate) solutions. Whole-cell current amplitude typically increased approximately two- to threefold and then stabilized within 1–2 min after obtaining the whole-cell configuration (Fig. 2 C).

The whole-cell current was voltage and time dependent (Fig. 2, A and B). Strong depolarization and hyperpolarization activated and inactivated the current, respectively. At +100 mV, current activation was well fit by a double exponential describing mean ± SEM fast (τ_f) and slow (τ_s) time constants of 19 ± 2 and 154 ± 29 ms (n = 43), respectively. Current inactivation was also well fit by a double exponential. Mean ± SEM τ_f and τ_s at −100 mV were 14 ± 2 and 195 ± 36 ms (n = 43), respectively.

The ionic nature of the outwardly rectifying whole-cell current was determined by ion substitution studies. Replacement of 147 mM Na^+ in the pipette solution with $NMDG^+$ dramatically inhibited outward current (Fig. 3 A) and increased E_{rev} significantly ($P < 0.005$) from a mean ± SEM value of 21 ± 3 (n = 5) to 37 ± 3 mV (n = 5).[1] The shift in E_{rev} and reduction in outward current are consistent with a cation current.

Reduction of bath Cl^- from 157 to 10 mM (gluconate replacement[2]) induced a small increase in outward current and shift in mean ± SEM E_{rev} from 29 ± 3 to 24 ± 1 mV (n = 3; Fig. 3 B). The small changes in current amplitude and E_{rev} induced by reduction of bath Cl^- were not statistically significant ($P > 0.1$) and are opposite to those expected for anion-selective channels. Taken together, the data in Fig. 3 demonstrate that the whole-cell current is carried predominantly by cations.

The Outwardly Rectifying Cation Conductance Has a High Selectivity for Ca^{2+} over Monovalent Cations

The relative permeability to various cations of the channel responsible for the outwardly rectifying whole-cell current was determined using the Goldman-Hodgkin-Katz equation after complete substitution of bath Na^+ with various test cations. Removal of bath Ca^{2+} and Mg^{2+} and addition of 1 mM EGTA (nominally divalent-free medium) caused an immediate and substantial increase in whole-cell current (Fig. 4). The mean ± SEM increase observed at +80 mV was 286 ± 58 pA (n = 27;

[1]The $NMDG^+$ pipette solution contained 3.5 mM CsOH and 5 mM Na^+ derived from 0.5 mM Na_2GTP and 2 mM Na_2ATP.

[2]Because gluconate is a strong calcium buffer, Ca^{2+} activity was measured with a calcium-sensitive electrode and adjusted to the same level present in NaCl bath.

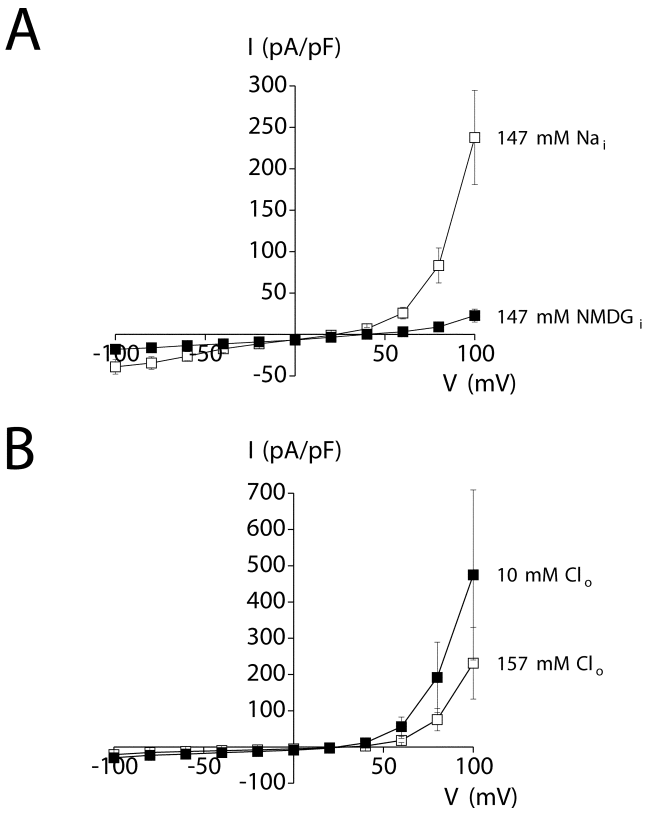

FIGURE 3. Ionic dependence of outwardly rectifying whole-cell current. (A) Replacement of 147 mM Na^+ (Na_i, □) in the pipette solution with $NMDG^+$ (■) increased reversal potential (E_{rev}) by +16 mV ($P < 0.005$) and dramatically reduced outward current.[1] Values are means ± SEM ($n = 5$). (B) Reduction of bath Cl^- concentration (Cl_o) from 157 (□) to 10 mM (■) (gluconate substitution) caused a small increase in outward current and decrease in E_{rev} of −3 ± 2 mV. The changes in current amplitude and E_{rev} were not statistically significant ($P > 0.1$). Values are means ± SEM ($n = 3$). Changes in E_{rev} and whole-cell current amplitude indicate that the current is carried primarily by cations. Voltage clamp protocol was the same as described in Fig. 2.

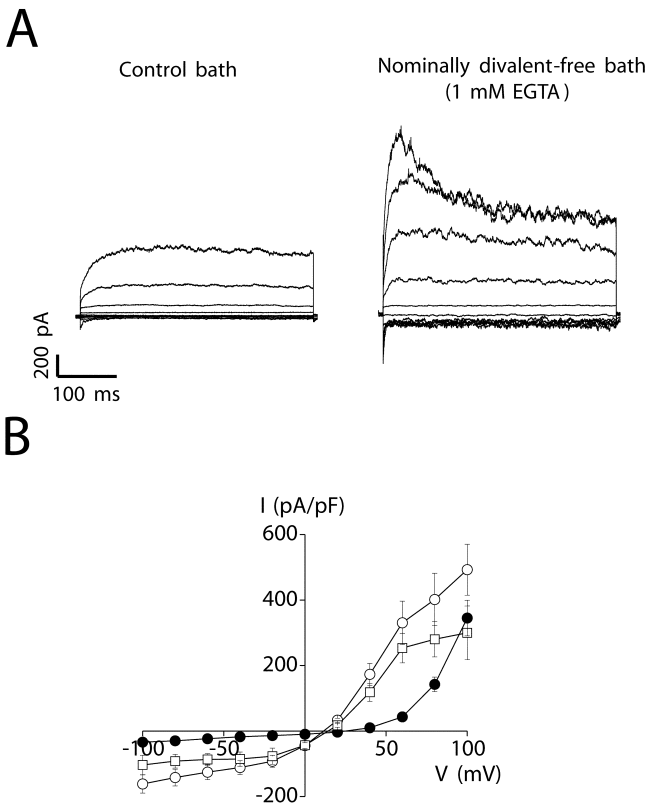

FIGURE 4. Effect of extracellular Ca^{2+} and Mg^{2+} removal on amplitude of the outwardly rectifying cation current. (A) Whole-cell currents observed under control (1 mM Ca^{2+} and 5 mM Mg^{2+}) and nominally divalent-free (0 mM Ca^{2+}, 0 mM Mg^{2+}, and 1 mM EGTA) conditions. Voltage clamp protocol was the same as described in Fig. 2. (B) Steady-state I–V relationships of outwardly rectifying currents observed under control conditions (●), in nominally divalent-free medium (buffered with 1 mM EGTA; ○) and in divalent-free medium (buffered with 1 mM EDTA; □). Values are means ± SEM ($n = 6$–33).

$P < 0.0001$). Removal of Ca^{2+} and Mg^{2+} also caused a significant ($P < 0.0001$) decrease in E_{rev}, from 24 ± 1 ($n = 48$) to 11 ± 0.5 mV ($n = 27$), and altered current voltage and time dependence (Fig. 4 A). At potentials of +80 mV and above, currents observed in nominally divalent-free medium typically showed partial inactivation (Fig. 4 A). Current inactivation was fit by a single exponential describing a mean ± SEM time constant (τ) at +100 mV of 194 ± 42 ms ($n = 17$).

Micromolar concentrations of extracellular Mg^{2+} block channels such as the NMDA receptor (Mayer et al., 1984; Nowak et al., 1984) and the recently described Mg^{2+}-inhibited cation (MIC) channel (Hermosura et al., 2002; Kozak et al., 2002). To determine whether a similar block occurs in the channel responsible for the outwardly rectifying cation current, we exposed cells to divalent-free medium containing 1 mM EDTA in order to fully chelate extracellular Mg^{2+}. As shown in Fig. 4 B, the current-to-voltage relationship of the outwardly rectifying current was largely unaffected by this maneuver.

Replacement of bath Na^+ with K^+, Cs^+, or $NMDG^+$ shifted E_{rev} to more negative values (Table I). The calculated relative permeabilities (i.e., P_{cation}/P_{Na}; Table I) determined from the changes in E_{rev} yielded a monovalent cation selectivity sequence of $Na^+ > K^+ > Cs^+ \gg NMDG^+$.

The increase in whole-cell current upon removal of extracellular divalent cations (Fig. 4) suggested strongly that the channel is permeable to Ca^{2+} and/or Mg^{2+} and that permeation by divalents blocks monovalent cation flux. To examine this possibility directly, we measured whole-cell currents in the presence of extracellular solutions containing varying proportions of Ca^{2+} and Na^+. Addition of 1 mM Ca^{2+} to a solution containing 74 mM Na^+ caused a dramatic reduction in whole-cell current (Fig. 5 A). As the proportion of Ca^{2+} was elevated, the current passed through a minimum

TABLE I

Relative Cation Permeability of the Outwardly Rectifying Conductance

Cation	ΔE_{rev}	P_{cation}/P_{Na}
	mV	
K^+	−10 ± 1	0.67 ± 0.02 (7)
Cs^+	−34 ± 2	0.27 ± 0.02 (7)
$NMDG^+$	−90 ± 5	0.03 ± 0.01 (7)
Ca^{2+}	29 ± 1	64 ± 2 (6)[a]

Whole-cell currents were elicited by stepping membrane voltage from −100 to +100 mV in 20-mV steps from a holding potential of 0 mV. Voltage steps were 400 ms long. Steady-state current-to-voltage relationships were plotted for determination of E_{rev} in the presence of Na^+ and various test cations. Relative permeabilities were calculated using equations derived from the Goldman-Hodgkin-Katz equation (see MATERIALS AND METHODS). Values are means ± SEM (number of cells). All changes in E_{rev} are statistically significant ($P < 0.0001$).

[a]See footnote 3.

and then increased (Fig. 5 A). This anomalous mole-fraction behavior is characteristic of multi-ion channels where two or more ions simultaneously occupy and move through the channel pore (Hille, 2001). Both the number and type of ions in the pore determine the overall permeability properties of multi-ion channels (Hille, 2001). Many highly Ca^{2+}-selective cation channels exhibit anomalous mole-fraction behavior (Hoth, 1995; Vennekens et al., 2001). High affinity Ca^{2+} binding in the channel pore appears to be responsible for their high selectivity for Ca^{2+} versus monovalent cations (Almers and McCleskey, 1984; Lepple-Wienhues and Cahalan, 1996).

Given the results in Fig. 4 and Fig. 5 A, we measured relative Ca^{2+} permeability by replacing bath Na^+ with 130 mM $NMDG^+$ and 10 mM Ca^{2+}. Elevation of bath Ca^{2+} increased E_{rev} significantly ($P < 0.0001$), by 29 ± 1 mV ($n = 6$) (Fig. 5 B; Table I). The calculated relative permeability of Ca^{2+} to Na^+ is 64:1 (Table I).[3] Together, the data in Figs. 4 and 5 demonstrate that a highly Ca^{2+}-selective cation channel carries the outwardly rectifying whole-cell current. We hereafter refer to the outwardly rectifying Ca^{2+} current as I_{ORCa}.

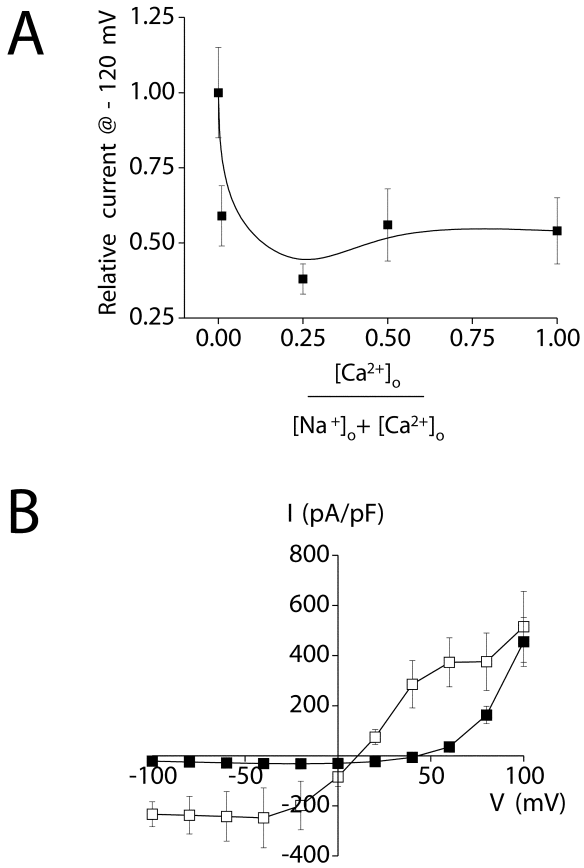

FIGURE 5. Calcium selectivity of the outwardly rectifying cation conductance. (A) Relationship between relative whole-cell current amplitude and fractional concentration of extracellular Ca^{2+} ($[Ca^{2+}]_o/([Na^+]_o + [Ca^{2+}]_o)$). As the proportion of Ca^{2+} is elevated, the current passes through a minimum and then increases. This anomalous mole-fraction behavior is characteristic of highly Ca^{2+}-selective cation channels (Hoth, 1995; Vennekens et al., 2001). All solutions were nominally Mg^{2+} free. The Ca^{2+}-free solution was buffered with 1 mM EGTA. Values are means ± SEM (n = 6–11). (B) I–V relationships of whole-cell current in the presence of 150 mM Na^+ in the bath (□) and when Na^+ was replaced with 130 mM $NMDG^+$ and 10 mM Ca^{2+} (■). Elevation of extracellular Ca^{2+} increased E_{rev} by 29 ± 1 mV ($P < 0.0001$). Calculated relative Ca^{2+} permeability (P_{Ca}/P_{Na}) is 64:1 (Table I). Voltage clamp protocol was the same as described in Fig. 2.

Pharmacological Characteristics of I_{ORCa}

Lanthanum is a trivalent cation that inhibits voltage-gated and store-operated Ca^{2+} channels as well as some members of the transient receptor potential (TRP) cation channel superfamily (Aussel et al., 1996; Halaszovich et al., 2000; Beedle et al., 2002). Exposure of cultured intestinal cells to 100 μM La^{3+} in the bath solution virtually abolished the outwardly rectifying current ($P < 0.05$; Fig. 6 A). Current inhibition by 100 μM La^{3+} was fully reversible (Fig. 6 A). The concentration of La^{3+} required for 50% inhibition of I_{ORCa} is 3.4 μM (Fig. 6 B).

SKF 96365 inhibits receptor-activated and voltage-gated calcium influx (Merritt et al., 1990) as well as the

[3]Removal of Ca^{2+} from the bath is likely to alter seal resistance. Changes in seal resistance would alter the magnitude of leak current and may affect estimates of P_{Ca}/P_{Na}. To assess the effect of leak on ORCa Ca^{2+} selectivity measurements, we patch clamped cells with a pipette solution containing 5 mM free Mg^{2+} to inhibit ORCa and 200 nM Ca^{2+} to prevent store depletion and I_{SOC} activation. Mean ($n = 4$) leak currents were estimated in bath solutions containing either 150 mM Na^+ or 130 mM $NMDG^+$ and 10 mM Ca^{2+}. Leak currents were subtracted from ORCa currents measured under the same conditions. The mean ± SEM shift in E_{rev} observed after replacement of bath Na^+ with $NMDG^+$ and Ca^{2+} was 29 ± 1 mV ($n = 6$) in the absence of leak subtraction versus 33 ± 1 mV ($n = 6$) after correction for leak. This small change was significant ($P < 0.02$) and increased the estimated P_{Ca}/P_{Na} from 64 ± 2 to 71 ± 2.

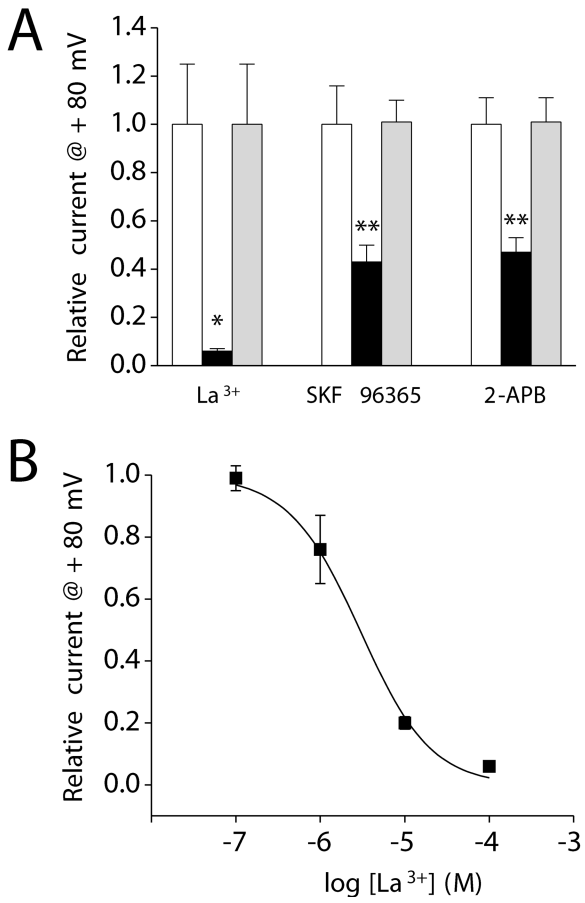

FIGURE 6. Pharmacology of the outwardly rectifying cation conductance. (A) Addition of 100 μM La^{3+}, 100 μM SKF 96365, or 100 μM 2-APB (black bar) to the bath inhibited whole-cell current by 50–90%. *, $P < 0.05$; **, $P < 0.01$ (compared with control, white bar). Inhibitory effects of La^{3+}, SKF 96365, and 2-APB were fully reversible. Current levels observed after drug washout (gray bar) were not significantly ($P > 0.05$) different from those observed before drug addition (white bar). Values are means ± SEM (n = 4–5). (B) Dose–response relationship for the inhibitory effect of La^{3+}. Data were fit using the equation $I = 1/1 + ([Mg^{2+}]/K_{1/2})^n$. $K_{1/2}$ and n are 3.4 μM and 1.1, respectively. Values are means ± SEM (n = 5–9). Voltage clamp protocol was the same as described in Fig. 2.

Ca^{2+} release–activated channel (CRAC) (Kozak et al., 2002; Prakriya and Lewis, 2002) and TRP channel activity (Halaszovich et al., 2000). 100 μM SKF 96365 inhibited I_{ORCa} ~60% ($P < 0.01$) in a reversible manner (Fig. 6 A). 2-APB inhibits IP_3 receptor Ca^{2+} channel activity (Bilmen and Michelangeli, 2002) and plasma membrane Ca^{2+} entry channels, including CRAC and TRP channels (Prakriya and Lewis, 2001; Bootman et al., 2002; Hermosura et al., 2002; Prakriya and Lewis, 2002). 100 μM 2-APB reversibly inhibited I_{ORCa} by ~50% ($P < 0.01$; Fig. 6 A). Lanthanum, SKF 96365, and 2-APB all inhibited I_{ORCa} rapidly; current inhibition was maximal within 30–60 s after adding the drugs to the bath (unpublished data). Washout of the drugs and recovery of I_{ORCa} occurred with a similar time course (unpublished data).

Depletion of Intracellular Ca^{2+} Stores Does Not Regulate I_{ORCa}

As shown in Fig. 2 C, I_{ORCa} activated two- to threefold during the first 1–2 min after obtaining whole-cell access. Two observations suggested that current activation might be due to depletion of intracellular Ca^{2+} stores. First, the biophysical characteristics of the current resemble those of members of the TRP cation channel superfamily. Evidence suggests that some TRPs may be regulated by store depletion (Clapham et al., 2001; Elliott, 2001; Montell, 2001; Zitt et al., 2002). Second, the pipette solutions used in the studies shown in Fig. 2 C contained 10 mM EGTA and low Ca^{2+}, which could lead to passive store depletion (Hoth and Penner, 1993).

We performed three experiments to directly examine the role of store depletion in regulation of I_{ORCa}. First, cells were patch clamped with a Ca^{2+}-free pipette solution to passively deplete stores or a solution containing 175 nM free Ca^{2+}. Calcium levels >90 nM are expected to maintain store Ca^{2+} levels (Hermosura et al., 2002; Kozak et al., 2002). As shown in Fig. 7 A, there was no significant ($P > 0.2$) difference in either the rate of current activation or the peak current amplitude observed in these two experiments.

Second, we patch clamped cells with a pipette solution containing 10 μM IP_3. Immediately after obtaining whole-cell access, IP_3-treated cells were exposed to a nominally divalent-free bath solution containing 1 μM thapsigargin to inhibit store Ca^{2+} uptake. Neither the rate of current activation nor the peak current amplitude were significantly ($P > 0.1$) altered by IP_3 and thapsigargin.

Finally, we attempted to activate I_{ORCa} in intact cells by depleting intracellular Ca^{2+} stores before patch clamping. Cells were incubated in nominally divalent-free bath solution containing 1 μM thapsigargin for 9–17 min and then were patch clamped with a pipette solution containing 10 μM IP_3. Control cells were patch clamped with a standard pipette solution without IP_3 and were exposed to nominally divalent-free bath immediately after obtaining whole-cell access. If store depletion activates I_{ORCa}, initial current levels should be higher in cells pretreated with Ca^{2+}- and Mg^{2+}-free bath containing thapsigargin. However, as shown in Fig. 7 C, initial whole-cell current amplitudes were not significantly ($P > 0.1$) different in control and experimental cells. The outward currents in both groups of cells showed gradual activation, but the rates of current activation and peak current amplitudes were not significantly ($P > 0.5$) different (Fig. 7 C). We conclude from the data shown in Fig. 7 that I_{ORCa} is not activated by depletion of intracellular Ca^{2+} stores.

I_{ORCa} Is Inhibited by Intracellular Mg^{2+}

We examined the effect of intracellular Mg^{2+} concentration on the activity of I_{ORCa}. Cells were patch

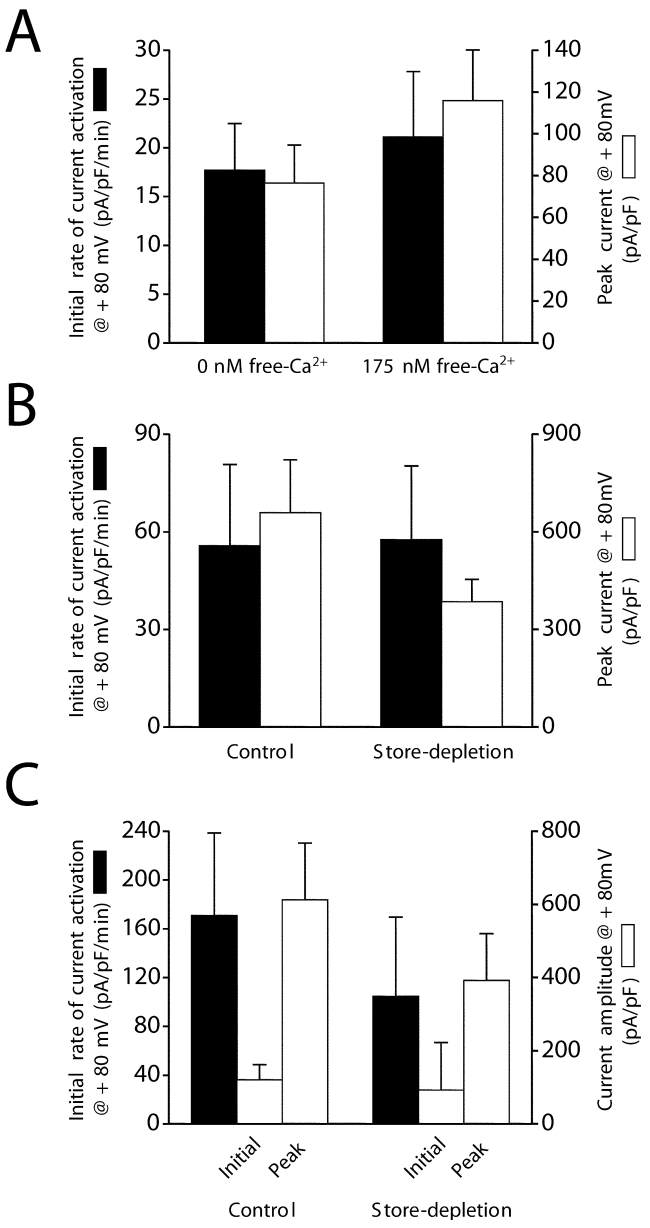

FIGURE 7. The outwardly rectifying cation current is not regulated by depletion of Ca^{2+} stores. (A) Rates of whole-cell current activation (black bar) and peak current amplitudes (white bar) in cells dialyzed with a Ca^{2+}-free pipette solution to passively deplete intracellular Ca^{2+} stores and a pipette solution containing 175 nM free Ca^{2+}. Removal of intracellular Ca^{2+} had no significant ($P > 0.2$) effect on the rate of current activation or the peak current amplitude. Intracellular Ca^{2+} was buffered with 1 mM EGTA. Currents were measured using the standard bath medium containing both Ca^{2+} and Mg^{2+}. Whole-cell currents were elicited by ramping membrane potential from −80 to +80 mV at 160 mV/s every 5 s. (B) Rates of whole-cell current activation (black bar) and peak current amplitudes (white bar) in control cells and cells treated with 10 μM IP_3 and 1 μM thapsigargin. Depletion of intracellular stores with IP_3 and thapsigargin had no significant ($P > 0.1$) effect on the rate of current activation or the peak current amplitude. Intracellular Ca^{2+} was buffered to 11 nM with 10 mM EGTA. Cells were exposed to nominally divalent-free bathing medium immediately after obtaining whole-cell access. Voltage clamp protocol was the same as described in Fig. 2. (C) Effect of depletion of Ca^{2+} stores in intact cells on rate of current activation (black bar) and initial and peak current amplitude (white bar). Experimental cells were preincubated for 9–17 min in nominally divalent-free bathing medium containing 1 μM thapsigargin and then patch clamped with a pipette solution containing 10 μM IP_3. Control cells were exposed to nominally divalent-free bathing medium immediately after obtaining whole-cell access and were not treated with IP_3 or thapsigargin. Store depletion had no significant ($P > 0.1$) effect on initial whole-cell current or subsequent current activation. Intracellular Ca^{2+} was buffered to 11 nM with 10 mM EGTA. Values are means ± SEM (n = 3–6). Voltage clamp protocol was the same as described in A. Initial rates of current activation were quantified by performing linear regression analysis on whole-cell currents measured during the first 60–180 s after obtaining whole-cell access.

clamped with an ATP- and GTP-free pipette solution in which EGTA was replaced by 10 mM BAPTA. The concentration of $MgCl_2$ added to the pipette solution varied between 0 and 6 mM. As shown in Fig. 8 (A and B), increasing free Mg^{2+} concentrations inhibited I_{ORCa} in a saturable manner. The estimated $K_{1/2}$ value for free Mg^{2+} is 692 μM (Fig. 8 B).

To determine if I_{ORCa} is also inhibited by Mg-nucleotides, 6 mM MgATP or 6 mM TrisATP was added to the pipette solution. As shown in Fig. 8 C, 6 mM MgATP inhibited whole-cell current ~60% at +80 mV ($P < 0.05$). The calculated free Mg^{2+} concentration in a solution containing 6 mM MgATP is 700 μM. When plotted as a function of calculated free Mg^{2+} concentration (Fig. 8 B, open circle), the degree of inhibition observed with 6 mM MgATP is very similar to that observed with Mg^{2+} alone. These results indicate that I_{ORCa} is inhibited by free Mg^{2+} but is insensitive to MgATP.

Intracellular Ca^{2+} Store Depletion Activates an Inwardly Rectifying Current

SOCCs play important roles in IP_3-dependent intracellular Ca^{2+} signaling pathways (Putney and McKay, 1999; Lewis, 2001; Taylor and Thorn, 2001). Given the dependence of the *C. elegans* defecation cycle on IP_3 and oscillatory Ca^{2+} signaling in the intestine (Dal Santo et al., 1999), we performed patch clamp studies to determine if intestinal cells expressed store-operated channels.

I_{ORCa}, which dominates whole-cell recordings, was inhibited by inclusion of 5 mM free Mg^{2+} in the pipette solution (Kozak et al., 2002; Prakriya and Lewis, 2002). To prevent Ca^{2+} store depletion, we patch clamped cells with a pipette solution containing ATP, GTP, and 200 nM free Ca^{2+} buffered with 10 mM BAPTA. The bath solution contained 145 mM Na^+ and 20 mM Ca^{2+}. Using these solutions, we observed that whole-cell current remained stable for at least 5–7 min after obtaining whole-cell access in three out of three cells (Fig. 9 C). The mean ± SEM current observed just before loss of the whole-cell seal was −5.5 ± 2.7 pA/pF at −120 mV (n = 3).

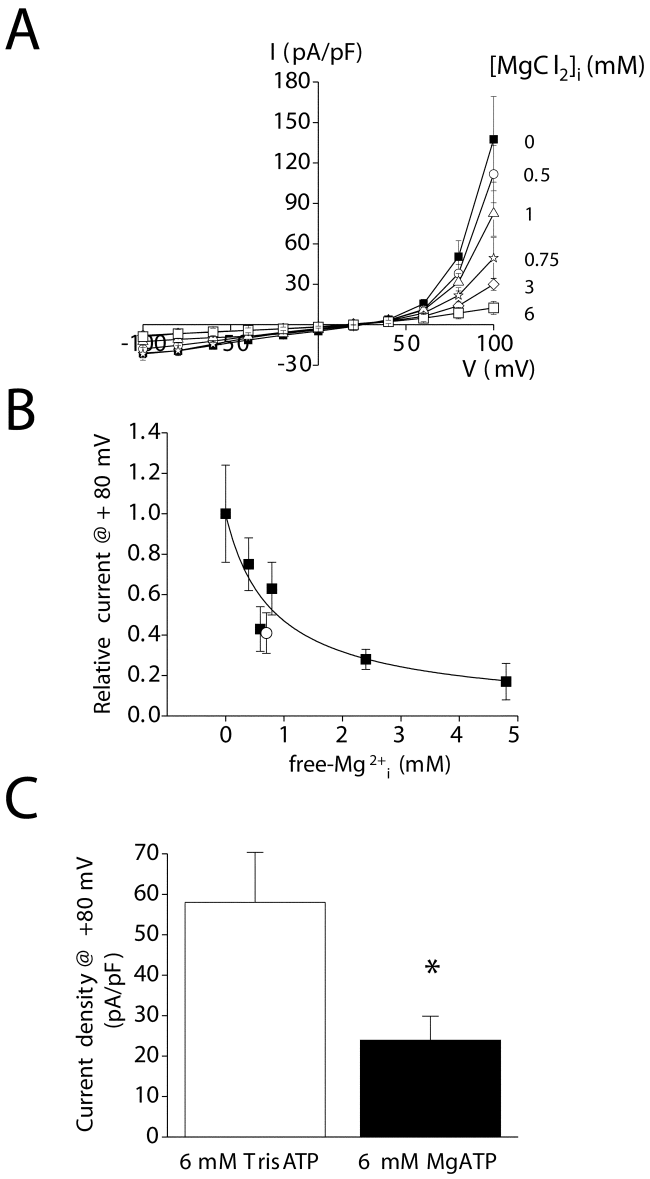

FIGURE 8. Inhibition of the outwardly rectifying cation current by intracellular Mg^{2+}. (A) I–V relationships for cells patch clamped with ATP- and GTP-free pipette solutions containing 0–6 mM $MgCl_2$. Chloride concentrations in the solutions were maintained constant by addition of 0–12 mM NMDGCl. EGTA was replaced with 10 mM BAPTA to buffer intracellular Ca^{2+} at 14 nM. Note that the Mg^{2+} concentrations indicated on the figure are those added to the pipette solution. Therefore, 0 Mg^{2+} should be considered nominally Mg^{2+} free. (B) Dose–response relationship for inhibition of the outwardly rectifying current by intracellular free Mg^{2+}. Data were fit using the equation $I = 1/1 + ([Mg^{2+}]/K_{1/2})^n$. $K_{1/2}$ and n are 692 μM and 0.8, respectively. Open circle is inhibition observed when free Mg^{2+} concentration is elevated by addition of 6 mM MgATP. (C) Effect of Mg^{2+} nucleotides on the outwardly rectifying cation current. Whole-cell current is inhibited ~60% by 6 mM MgATP. Calculated concentration of free Mg^{2+} in the pipette solution containing 6 mM MgATP is 700 μM. The degree of inhibition is similar to that observed when free Mg^{2+} is elevated by addition of $MgCl_2$ (see B). *, $P < 0.05$ (compared with 6 mM TrisATP). Values are means ± SEM (n = 5–9). Currents were measured in standard bath medium containing both Ca^{2+} and Mg^{2+} 3–4 min after obtaining whole-cell access when activation was complete. Voltage clamp protocol was the same as described in

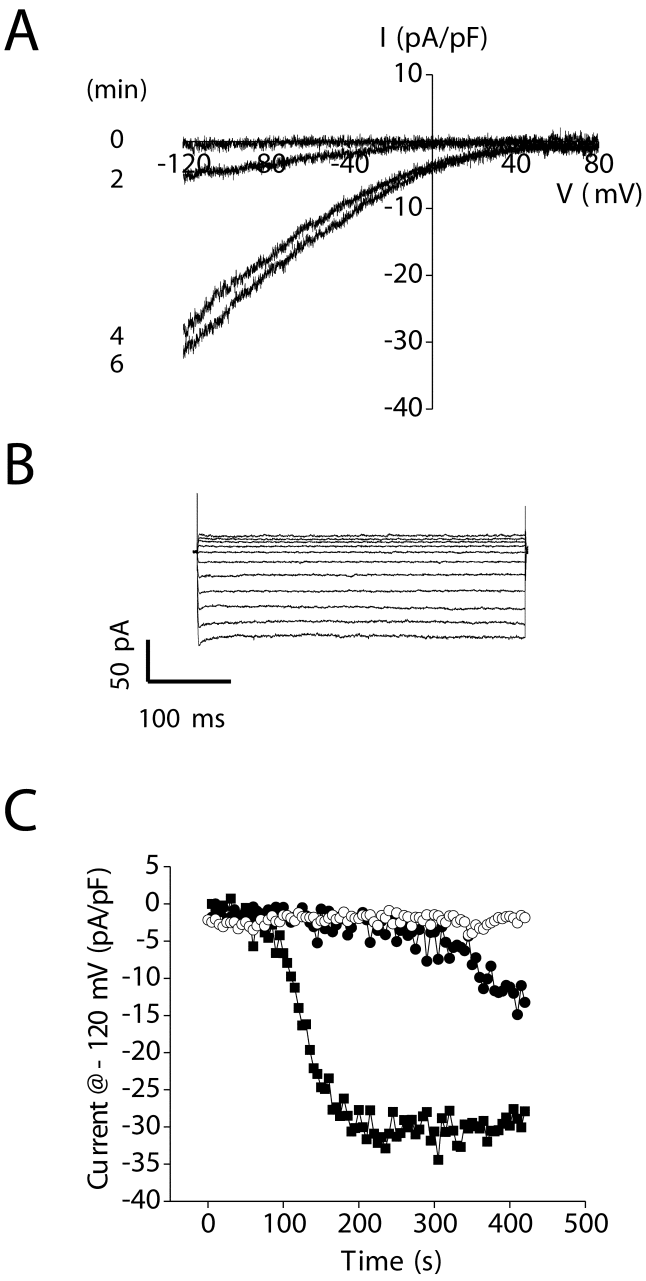

FIGURE 9. Activation of an inwardly rectifying store-operated current by depletion of intracellular Ca^{2+} stores. (A) An inwardly rectifying current activates when store depletion is induced by addition of 10 μM IP_3 to a pipette solution containing 18 nM free Ca^{2+}. Currents were elicited by ramping membrane voltage from −120 to +80 mV at 200 mV/s every 5 s. Leak current was subtracted from the traces shown. (B) Inwardly rectifying whole-cell currents elicited by stepping membrane voltage from −120 to +80 mV from a holding potential of 0 mV. Steps were 400 ms in duration. Currents were measured after activation induced by IP_3 was complete. (C) Changes in whole-cell current observed in the absence of store depletion (○), during passive store depletion (●), and during active store depletion induced by IP_3 (■). Leak current was subtracted from the currents induced by active and passive store depletion. All experiments shown were performed in the presence of 5 mM free Mg^{2+} in the pipette solution to inhibit I_{ORCa} and 145 mM Na^+/20 mM Ca^{2+} in the bath.

TABLE II

Store Depletion–induced Activation Characteristics of the Inwardly Rectifying Current

Store depletion protocol	Time to start of current activation[a]	Rate of current activation[b]	Time to peak current	Peak current
	s	*pA/pF/min*	*s*	*pA/pF*
Passive	163 ± 26 (8)	−3.3 ± 0.5 (8)	462 ± 52 (6)	−16 ± 3 (6)
Active				
10 μm IP_3	84 ± 12[c] (81)	−26 ± 3[e] (81)	230 ± 17[d] (77)	−31 ± 2[d] (77)
Active				
2 μm ionomycin		−72 ± 17[e] (8)		−38 ± 14 (8)

Currents were elicited by ramping membrane voltage from −120 to +80 mV at 200 mV/s every 5 s. Peak current and rate of current activation were measured at −120 mV.

[a]Time to start of current activation is the time after obtaining whole-cell access that current activation began.

[b]Rate of current activation was quantified by performing linear regression analysis on whole-cell currents measured during the first 60–120 s after initiation of current activation. The time course of current activation in many cells was sigmoidal in nature (e.g., Fig. 9 C), displaying an initial very slowly rising phase followed by a much steeper and rapid linear increase in current amplitude. To avoid ambiguity in characterizing current activation, we measured the rate of activation during the steepest initial part of this sigmoidal curve. The first point to fall within this region was defined as the start of current activation. Values are means ± SEM (number of cells).

[c]$P < 0.05$, compared with passive store depletion.

[d]$P < 0.01$, compared with passive store depletion.

[e]$P < 0.001$, compared with passive store depletion.

Active depletion of Ca^{2+} stores was induced by dialyzing cells with a nucleotide-free pipette solution containing 18 nM free Ca^{2+} and 10 μM IP_3. A strongly inwardly rectifying, voltage-independent cation current was activated under these conditions (Fig. 9, A–C). The mean time to the start of current activation after membrane rupture was 84 s, and the current activated to a peak value of −31 pA/pF at −120 mV at an initial rate of −26 pA/pF/min (Table II).

It is conceivable that the inwardly rectifying current is activated by IP_3 rather than store depletion per se. To test for this possibility, we passively depleted intracellular Ca^{2+} stores by dialyzing cells with a pipette solution containing 18 nM free Ca^{2+} alone. Passive store depletion also activated an inwardly rectifying current (Fig. 9 C), albeit at a rate ~13% of that observed when stores were depleted actively. The mean time to the start of current activation after membrane rupture was 163 s (Table II). This delay in current activation was significantly ($P < 0.05$) longer than that observed in the presence of IP_3 (Table II). Mean initial rate of current activation and peak current at −120 mV were −3.3 pA/pF/min and −16 pA/pF, respectively (Table II). The rate of current activation and peak current were significantly ($P < 0.01$) decreased compared with that observed with active store depletion induced by IP_3 (Table II). These results are consistent with store depletion being the mechanism responsible for activation of the inwardly rectifying current.

As a final test for the involvement of store depletion in current activation, we dialyzed cells with a pipette solution containing 18 nM free Ca^{2+} and then exposed them 30–150 s after obtaining whole-cell access to 2 μM ionomycin for 30–60 s. Ionomycin is a Ca^{2+} ionophore that is expected to induce efflux of Ca^{2+} from intracellular stores and activation of store-dependent cation channels (Hoth and Penner, 1993; Parekh, 1998; Voets et al., 2001). In the presence of ionomycin, the inwardly rectifying current activated rapidly. The initial rate of current activation and peak current in the presence of ionomycin were −72 pA/pF/min and −38 pA/pF, respectively, at −120 mV. The rate of current activation was ~22-fold faster ($P < 0.001$) than that observed with passive store depletion (Table II). Taken together, the results shown in Fig. 9 and Table II demonstrate clearly that depletion of IP_3-dependent intracellular Ca^{2+} stores activates an inwardly rectifying store-operated current. Currents activated by the three store depletion protocols had the same I–V relationships (unpublished data), indicating that they were likely carried by the same channel.

Selectivity of the Store-operated Channel

In the presence of 145 mM Na^+ and 20 mM Ca^{2+} in the bath, the store-operated current showed very strong inward rectification (Fig. 9, A and B) and voltage-independent gating (Fig. 9 B). For the majority of cells examined, the slope of the I–V plot at positive voltages was extremely shallow, and a clear reversal of current direction was not detectable (Fig. 9 A).

Replacement of bath Na^+ and Ca^{2+} with $NMDG^+$ completely blocked inward current (Fig. 10 A), demonstrating that the channel is highly cation selective. In the presence of 130 mM $NMDG^+$ and 10 mM Ca^{2+}, a strongly inwardly rectifying current was observed (Fig. 10 A). Mean ± SEM current density at −120 mV was −31 ± 5 pA/pF ($n = 4$), which is similar to that observed in the presence of Na^+ and Ca^{2+} (Table II). These results demonstrate that the store-operated channel has a high selectivity for Ca^{2+} or Na^+. The inability to accurately measure E_{rev} at positive voltages precludes accurate calculation of relative Ca^{2+} to Na^+

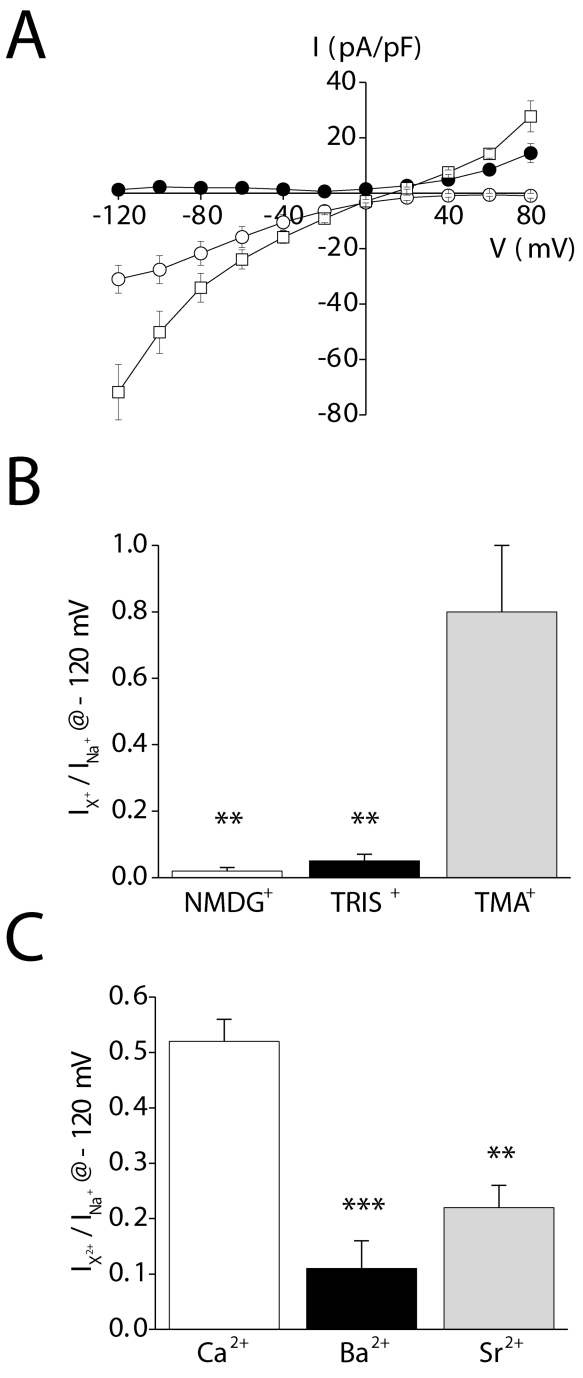

FIGURE 10. Cation selectivity of the inwardly rectifying current. (A) Whole-cell currents observed in the presence of various extracellular cations. Exposure of cells to divalent-free (buffered with 1 mM EDTA) 150 mM Na^+ bath increases inward and outward monovalent current (□; compare with Fig. 9 A). Replacement of bath Na^+ with 150 mM $NMDG^+$ (●) eliminates inward current. In the presence of 10 mM Ca^{2+} and 130 mM $NMDG^+$ (○), inward current is restored. (B) Relative organic cation currents (i.e., I_{cation}/I_{Na}). Whole-cell currents were measured at −120 mV in divalent-free (buffered with 1 mM EDTA) 150 mM Na^+-containing bath and after complete replacement of Na^+ with various organic cations. **, $P < 0.01$ (compared with current observed with Na^+). (C) Relative divalent cation currents (i.e., $I_{divalent}/I_{Na}$). Whole-cell currents were measured at −120 mV in a divalent-free (buffered with 1 mM EDTA) 150 mM Na^+-containing bath and in a bath containing 130 mM $NMDG^+$ and 10 mM Ca^{2+}, Ba^{2+}, or Sr^{2+}. **, $P < 0.01$; ***, $P < 0.001$ (compared with current observed with Ca^{2+}). Values are means ± SEM (n = 4–13). Whole-cell currents were elicited by stepping membrane voltage from −120 to +80 mV from a holding potential of 0 mV. Steps were 400 ms in duration. Whole-cell current was activated by inclusion of 10 μM IP_3 in the patch pipette solution. Leak currents were subtracted from all current records. Experiments were performed in the presence of 5 mM free Mg^{2+} in the pipette solution to inhibit I_{ORCa}.

TABLE III

Relative Inorganic Monovalent Cation Permeability of the Inwardly Rectifying Conductance

Cation	ΔE_{rev}	P_{cation}/P_{Na}
	mV	
Li^+	1.4 ± 0.9	1.06 ± 0.04 (5)
Cs^+	−16 ± 5[a]	0.60 ± 0.10 (7)
Rb^+	−16 ± 4[b]	0.57 ± 0.08 (6)

Whole-cell currents were elicited by stepping membrane voltage from −120 to +80 mV in 20-mV steps from a holding potential of 0 mV. Voltage steps were 400 ms long. Steady-state current-to-voltage relationships were plotted for determination of E_{rev} in the presence of Na^+ and various test cations. Relative permeabilities were calculated using equations derived from the Goldman-Hodgkin-Katz equation (see MATERIALS AND METHODS). Values are means ± SEM (number of cells).

[a] $P < 0.03$.

[b] $P < 0.02$.

permeability. However, if E_{rev} is >+80 mV, the estimated P_{Ca}/P_{Na} is >1,000:1. Based on these results, we hereafter refer to the inwardly rectifying store-operated Ca^{2+} channel as SOCC and the channel current as I_{SOC}.

In the presence of divalent-free (buffered with 1 mM EDTA) 150 mM Na^+-containing bath, significant inward and outward current was detected (Fig. 10 A). Mean ± SEM E_{rev} of the Na^+ current was 13 ± 1 mV (n = 28). Replacement of bath Na^+ with Cs^+ or Rb^+ shifted E_{rev} to more negative values (Table III). Substitution of Na^+ with Li^+ had no significant ($P > 0.2$) effect on E_{rev} (Table III). The calculated relative cation permeabilities (i.e., P_{cation}/P_{Na}; Table III) determined from the changes in E_{rev} yielded a monovalent inorganic cation selectivity sequence of $Na^+ \approx Li^+ > Rb^+ \approx Cs^+$.

We attempted to measure relative organic cation permeability of SOCC by replacing bath Na^+ with TMA^+, $TRIS^+$, or $NMDG^+$. Reversal potentials could not be accurately estimated for $NMDG^+$ and $TRIS^+$. We therefore quantified organic cation current relative to Na^+ current (i.e., I_{cation}/I_{Na}) at −120 mV. TMA^+ and $TRIS^+$ currents were ~80 and 5%, respectively, of those observed with Na^+; $NMDG^+$ was effectively impermeant (Fig. 10, A and B). The diameters of TMA^+, $TRIS^+$, and $NMDG^+$ are 0.55 nm, 0.64 nm, and 0.68 nm, respectively (Hille, 2001). This suggests that the pore diameter of SOCC is ~0.6–0.7 nm.

To determine whether the observed organic solute permeabilities are reflective of SOCC rather than nonspecific leak, we measured TMA^+ and $TRIS^+$ currents relative to Na^+ in the absence of store depletion and I_{SOC} activation. Mean ± SEM I_{cation}/I_{Na} for TMA^+ and $TRIS^+$ were 1.0 ± 0.2 (n = 5) and 1.6 ± 0.9 (n = 6), respectively. These values were not significantly different ($P > 0.6$), indicating that the leak does not discriminate between the two cations. In contrast, SOCC discriminates strongly between TMA^+ and $TRIS^+$ (Fig. 10 B).

We also attempted to measure relative divalent cation permeability of the channel. Cells were bathed initially with a divalent-free solution containing 150 mM Na^+. Sodium was then replaced by a solution containing 130 mM $NMDG^+$ and 10 mM Ca^{2+}, Ba^{2+}, or Sr^{2+}. Relative divalent cation currents (i.e., $I_{divalent}/I_{Na}$) at −120 mV are shown in Fig. 10 C. Both Ba^{2+} and Sr^{2+} were significantly ($P < 0.01$) less permeable than Ca^{2+}. The divalent cation selectivity sequence of SOCC is $Ca^{2+} > Ba^{2+} \approx Sr^{2+}$.

Pharmacological Characteristics of I_{SOC}

We compared the pharmacological properties of I_{SOC} to I_{ORCa}. Exposure of intestinal cells to 100 μM La^{3+} inhibited I_{SOC} ~90% ($P < 0.01$; Fig. 11, A and B). This inhibitory effect was partially reversible (Fig. 11 A). The concentration of La^{3+} required to inhibit I_{SOC} 50% was 9 μM (Fig. 11 B), a value twofold higher than that observed for I_{ORCa} (Fig. 6 A).

100 μM SKF 96365 inhibited I_{SOC} ~65% ($P < 0.01$) in a reversible manner (Fig. 11 A). Concentrations of 2-APB >10 μM irreversibly inhibit CRAC (Prakriya and Lewis, 2001, 2002; Voets et al., 2001; Hermosura et al., 2002). However, at lower concentrations (5 μM), the drug stimulates CRAC activity (Prakriya and Lewis, 2001, 2002). The intestinal cell SOCC has some characteristics that resemble those of CRAC (see DISCUSSION). We therefore tested the effects of low and high concentrations of 2-APB on the current. Exposure to 5 μM 2-APB had no significant ($P > 0.05$) effect on I_{SOC} (Fig. 11 A). Washout of the drug induced a small, but statistically significant ($P < 0.05$), increase in current. Exposure to 100 μM 2-APB inhibited I_{SOC} by ~90% (Fig. 11 A). Inhibition was completely reversed by drug washout (Fig. 11 A).

Inactivation of I_{SOC}

I_{SOC} activity was relatively stable in the presence of a bath solution containing 145 mM Na^+ and 20 mM Ca^{2+} (Fig. 12 A). Mean ± SEM relative current observed 3 min after store depletion–induced activation was complete was 0.93 ± 0.02 (n = 18). In contrast, the SOCC-mediated Na^+ current observed in divalent-free bath inactivated immediately after Ca^{2+} removal (Fig. 12 B). The mean ± SEM rate of Na^+ current inactivation was −12 ± 2 pA/pF/min or −13 ± 2%/min (n = 9).

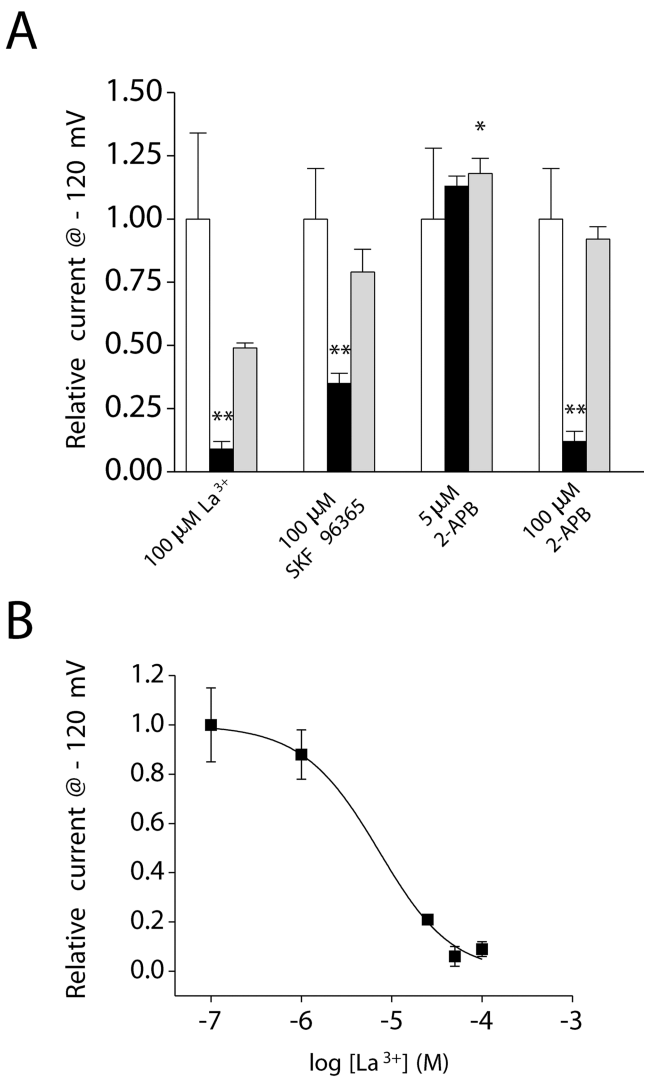

FIGURE 11. Pharmacology of the inwardly rectifying current. (A) Addition of 100 μM La^{3+}, 100 μM SKF 96365, or 100 μM 2-APB (black bar) to the bath inhibited whole-cell current by 65–90%. *, $P < 0.05$; **, $P < 0.01$ (compared with control, white bar). 5 μM 2-APB had no effect on whole-cell current (black bar). Inhibitory effects of SKF 96365 and 2-APB were fully reversible (gray bar). Current levels observed after washout of SKF 96365 and 100 μM 2-APB (gray bar) were not significantly ($P > 0.05$) different from those observed before drug addition (white bar). Washout of 5 μM 2-APB caused a small but significant (*, $P < 0.05$) stimulation of whole-cell current. Values are means ± SEM (n = 4–6). (B) Dose–response relationship for the inhibitory effect of La^{3+}. Data were fit using the equation $I = 1/1 + ([Mg^{2+}]/K_{1/2})^n$. $K_{1/2}$ and n are 9 μM and 1.2, respectively. Values are means ± SEM (n = 4–8). Voltage clamp protocol was the same as described in Fig. 9 B. Whole-cell current was activated by inclusion of 10 μM IP_3 in the patch pipette solution. Leak currents were subtracted from all current records. Experiments were performed in the presence of 5 mM free Mg^{2+} in the pipette solution to inhibit I_{ORCa} and 145 mM Na^+/20 mM Ca^{2+} in the bath.

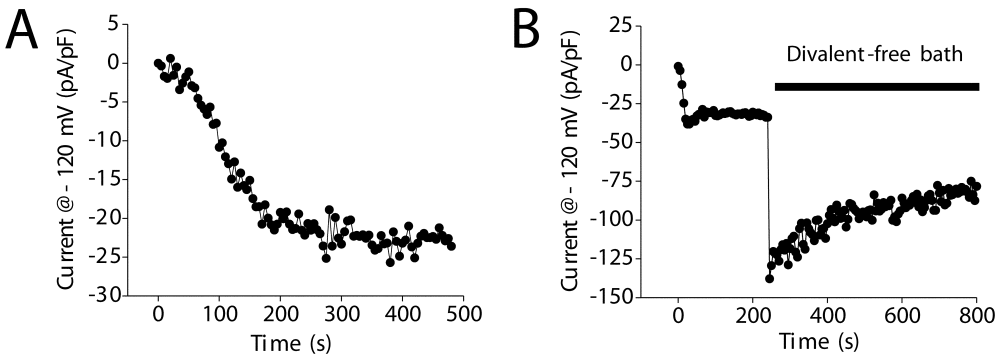

FIGURE 12. Inactivation of the inwardly rectifying current. (A) Example of active store depletion–induced activation of whole cell in a bath solution containing 145 mM Na^+ and 20 mM Ca^{2+}. Pipette solution contained 10 μM IP_3 and 18 nM free Ca^{2+}. Current remains stable after store depletion–induced activation is complete. (B) Effect of divalent-free (buffered with 1 mM EDTA) bath solution on whole-cell current. Current was activated by active store depletion with 10 μM IP_3. Sodium current begins to inactivate immediately after removal of divalent cations from the bath. Voltage clamp protocol was the same as described in Fig. 9 A. Leak currents were subtracted from all current records. Experiments were performed in the presence of 5 mM free Mg^{2+} in the pipette solution to inhibit I_{ORCa}.

DISCUSSION

Functional Properties of C. elegans Intestinal Epithelial Cell Ca^{2+} Conductances

The *C. elegans* intestine provides a unique model system in which to characterize the molecular details of IP_3-dependent oscillatory Ca^{2+} signaling. To begin defining the functional roles and regulation of cation channels involved in Ca^{2+} signaling events, we performed patch clamp analysis of intestinal cells cultured in vitro (Christensen et al., 2002). Intestinal epithelial cells develop and survive in culture (Fig. 1) and are present at a frequency similar to that observed in newly hatched L1 larvae (see RESULTS).

Our initial patch clamp studies on intestinal cells were performed using "physiological" bath (5 mM K^+ and 145 mM Na^+) and pipette (143 mM K^+ and 4 mM Na^+) solutions described originally by Lockery and coworkers (Goodman et al., 1998). Under these conditions, whole-cell current showed strong outward rectification (unpublished data). Ion substitution studies demonstrated that an outwardly rectifying cation channel carries this current (Figs. 2–4; Table I). The channel conducts both monovalent and divalent cations and has high selectivity for Ca^{2+} over Na^+ (P_{Ca}/P_{Na} = 64:1; Table I). Lanthanum, 2-APB, and SKF 96365 reversibly inhibited the current (Fig. 6), and intracellular Mg^{2+} inhibited channel activity with a $K_{1/2}$ of 692 μM (Fig. 8).

The outwardly rectifying Ca^{2+} current (I_{ORCa}) was constitutively active in all cells examined. Currents typically increased two to threefold after whole-cell access was obtained. Activation is not mediated by depletion of intracellular Ca^{2+} stores (Fig. 7). Channel activation may be mediated by washout of intracellular Mg^{2+}, changes in protein phosphorylation, and/or other as yet undefined mechanisms.

I_{ORCa} shares some characteristics with MIC, Mg^{2+}-nucleotide–regulated metal ion (MagNuM), and TRPM7 currents. These shared characteristics include cation selectivity, permeability to Ca^{2+}, strong outward rectification, gradual activation after obtaining whole-cell access, and insensitivity to store depletion (Nadler et al., 2001; Hermosura et al., 2002; Kozak et al., 2002; Prakriya and Lewis, 2002). Importantly, the degree of inhibition of ORCa by Mg^{2+} is similar to that of the recently described MIC/MagNuM currents in RBL and Jurkat T cells (Hermosura et al., 2002; Kozak et al., 2002; Prakriya and Lewis, 2002).

TRPM7 and/or other TRP genes have been proposed to encode MIC/MagNuM (Nadler et al., 2001; Clapham, 2002; Prakriya and Lewis, 2002). The biophysical similarities between MIC/MagNuM and ORCa suggest that the channels may have a common molecular origin. However, there are also a number of significant differences between the channel types. For example, removal of extracellular Mg^{2+} and Ca^{2+} causes the I–V relationship to become linear for MIC, MagNuM, and TRPM7 (Nadler et al., 2001; Hermosura et al., 2002; Kozak et al., 2002; Prakriya and Lewis, 2002), but does not alter I_{ORCa} rectification (Fig. 4). I_{ORCa} shows voltage- and time-dependent gating (Fig. 4), whereas gating of TRPM7 is largely voltage insensitive (Runnels et al., 2001). MIC, MagNuM, and TRPM7 discriminate poorly between Ca^{2+} and Na^+ (Nadler et al., 2001; Runnels et al., 2001) and Cs^+ and Na^+ ($P_{Cs}/P_{Na} \approx 1$) (Runnels et al., 2001; Kozak et al., 2002; Prakriya and Lewis, 2002). In contrast, I_{ORCa} is highly selective for Ca^{2+} over Na^+ and P_{Cs}/P_{Na} is 0.27 (Table I). Finally, Na^+ current through ORCa is half blocked by ~1 mM Ca^{2+} (Fig. 5 A), whereas MIC is half blocked by <5 μM Ca^{2+} (Kerschbaum and Cahalan, 1998). Studies focused on identifying the gene or genes that encode ORCa are currently underway.

Given the role of IP_3 and Ca^{2+} signaling in regulating defecation rhythm in *C. elegans* (Dal Santo et al., 1999), we performed a series of studies to determine whether

intestinal cells also express SOCCs. To observe SOCC activity, we inhibited I_{ORCa} by addition of millimolar concentrations of free Mg^{2+} (Hermosura et al., 2002; Kozak et al., 2002) to the patch pipette solution.

In the absence of store depletion, whole-cell current was stable (Fig. 9 C). Active or passive depletion of Ca^{2+} stores activated a strongly inwardly rectifying current (Fig. 9, A and B). When stores were depleted actively by inclusion of 10 μM IP_3 in the patch pipette solution or by addition of 2 μM ionomycin to the bath, the rates of current activation were increased ~8- and ~22-fold compared with passive store depletion (Fig. 9 C; Table II). These results demonstrate clearly that Ca^{2+} store depletion activates an inwardly rectifying store-operated channel.

The inwardly rectifying channel is highly cation selective. Inward current was undetectable when bath Na^+ and Ca^{2+} were replaced by $NMDG^+$ (Fig. 10 A). Addition of Ca^{2+} to an NMDGCl bath solution induced inward current with an amplitude similar to that observed with Na^+ and Ca^{2+} (Fig. 9 A; Fig. 10 A; Table II). In a divalent-free Na^+-containing bath, E_{rev} was 13 mV (Fig. 10 A). Addition of 20 mM Ca^{2+} shifted E_{rev} to more positive potentials. However, it was not possible to measure E_{rev} accurately under these conditions because the slope of the I–V plot from 0 to +80 mV was extremely shallow (Fig. 9 A). Nevertheless, these results demonstrate that the store-operated channel is highly selective for Ca^{2+} over monovalent cations. If $E_{rev} >$ +80 mV, the channel would have a Ca^{2+} to Na^+ selectivity of at least 1,000:1.

CRAC is the most extensively characterized SOCC and is probably expressed ubiquitously in vertebrate cells (Parekh and Penner, 1997). The intestinal cell SOCC shares a number of characteristics with CRAC, including activation by passive and active store depletion, very strong inward rectification, and an apparent high selectivity for Ca^{2+} over monovalent cations (Hoth and Penner, 1993). Cation selectivity sequences of CRAC vary somewhat between cell types and are possibly altered by intracellular Ca^{2+} buffering (Zhang and McCloskey, 1995; Fierro and Parekh, 2000). Hoth and Penner (1992) and Zweifach and Lewis (1993) reported a CRAC divalent cation selectivity sequence of $Ca^{2+} > Ba^{2+} \approx Sr^{2+}$ in mast and Jurkat T cells. In RBL cells, Fierro and Parekh (1999) reported a slightly different divalent cation selectivity sequence of $Ca^{2+} > Sr^{2+} > Ba^{2+}$. The selectivity sequence observed in mast and T cells is similar to that of the intestinal cell SOCC (Fig. 10 C).

CRAC monovalent cation selectivity sequences of $Na^+ \approx Li^+ > K^+ > Cs^+$ (Voets et al., 2001) and $Na^+ \approx Li^+ > Rb^+ > Cs^+$ (Bakowski and Parekh, 2002) have been observed in RBL cells. In T cells, Lepple-Wienhues and Cahalan (1996) reported a monovalent cation selectivity for CRAC of $Na^+ > Li^+ = K^+ > Rb^+ \gg Cs^+$. The monovalent selectivity sequence for the intestinal cell SOCC is $Na^+ \approx Li^+ > Rb^+ \approx Cs^+$ (Table III) and resembles that reported for RBL cells (Voets et al., 2001; Bakowski and Parekh, 2002). The most significant difference in CRAC and SOCC cation selectivity is their relative Cs^+ permeabilities. CRAC has a P_{Cs}/P_{Na} of ~0.1, whereas P_{Cs}/P_{Na} for SOCC is 0.6 (Table III).

TMA^+ permeated SOCC nearly as well as Na^+, whereas $TRIS^+$ and $NMDG^+$ had very low or negligible permeability (Fig. 10, A and B), suggesting that the channel has a minimum pore diameter of ~0.6–0.7 nm. TMA^+ permeation through CRAC in RBL cells is undetectable, and a pore diameter of 0.32–0.55 nm has been estimated (Bakowski and Parekh, 2002). In Jurkat T cells, TMA^+ permeates CRAC, albeit poorly (Kerschbaum and Cahalan, 1998). Kerschbaum and Cahalan (1998) have estimated a minimum pore diameter for the T cell CRAC of at least 0.58 nm.

When exposed to divalent-free Na^+ medium, CRAC undergoes a rapid inactivation (Christian et al., 1996; Lepple-Wienhues and Cahalan, 1996; Voets et al., 2001; Kozak et al., 2002; Prakriya and Lewis, 2002). In Jurkat T cells for example, CRAC activity declines up to ~80% within ~20 s after removal of bath Ca^{2+} (Prakriya and Lewis, 2002). Inactivation of CRAC may reflect extracellular Ca^{2+}-dependent changes in channel gating (Zweifach and Lewis, 1995; Christian et al., 1996).

The *C. elegans* SOCC also inactivates in divalent-free medium (Fig. 12). However, this inactivation is considerably slower than that observed with CRAC. The SOCC-mediated Na^+ current inactivates at a rate of −13%/min.

At present, it is not possible to conclude that homologous genes encode CRAC and the intestinal SOCC because the molecular identities of both channels are unknown. However, *C. elegans* clearly provides unique experimental advantages and opportunities for identifying SOCC-encoding genes. Identification of these genes may ultimately provide clues into the molecular identity of CRAC.

Role of Store-independent and Store-operated Ca^{2+} Channels in Oscillatory Ca^{2+} Signaling

Extracellular agonist–induced Ca^{2+} signaling in nonexcitable cells requires the release of Ca^{2+} from IP_3-regulated intracellular stores and the influx of Ca^{2+} across the plasma membrane via SMOCCs and SOCCs (Elliott, 2001; Zitt et al., 2002). High concentrations of agonists typically trigger sustained elevation of cytoplasmic Ca^{2+} levels. It is generally accepted that SOCCs play important roles in maintaining globally elevated Ca^{2+} concentrations and in refilling depleted Ca^{2+} stores (Parekh and Penner, 1997; Elliott, 2001). However, in the presence of lower, physiologically relevant agonist concentrations, Ca^{2+} changes are more com-

plex, occurring in oscillations and waves and in localized areas of the cell (Shuttleworth, 1999; Berridge et al., 2000). The mechanisms responsible for generating Ca^{2+} oscillations are varied and depend on passive Ca^{2+} buffering, the spatial distribution of Ca^{2+} stores, rates of Ca^{2+} transport across the plasma membrane, and mitochondrial and ER Ca^{2+} uptake (Shuttleworth, 1999; Berridge et al., 2000; Bootman et al., 2001; Petersen, 2002). The specific roles played by SMOCCs and SOCCs in oscillatory Ca^{2+} signaling are unclear. Calcium oscillations in some cell types continue for long periods in the absence of extracellular Ca^{2+} (Lechleiter and Clapham, 1992), whereas oscillatory Ca^{2+} signals in other cell types are strictly dependent on Ca^{2+} influx (Torihashi et al., 2002; Wu et al., 2002).

Dolmetsch and Lewis (1994) have proposed that Ca^{2+} oscillations in T lymphocytes are driven primarily by pulsatile Ca^{2+} influx via CRAC. These investigators suggest that the main function of the intracellular Ca^{2+} stores is to control the extent and timing of CRAC activity (Dolmetsch and Lewis, 1994). Pharmacological studies in rat hepatocytes (Gregory and Barritt, 2003) and astrocytes (Pizzo et al., 2001) also suggest that Ca^{2+} oscillations are dependent on CRAC-mediated Ca^{2+} influx.

Shuttleworth and coworkers (Shuttleworth, 1999; Mignen et al., 2003) have noted that evidence for the involvement of CRAC specifically and SOCCs in general in generating Ca^{2+} oscillations is limited. Shuttleworth has also argued that CRAC possesses neither the sensitivity to store depletion nor the activation kinetics required for oscillatory Ca^{2+} signaling (Shuttleworth, 1999). Instead, he has suggested that the function of CRAC may be primarily to mediate plasma membrane Ca^{2+} influx required for refilling ER stores under conditions of sustained store depletion (Shuttleworth, 1999).

Recently, an arachidonic acid–regulated Ca^{2+} channel (ARC) has been described in many cell types (Mignen and Shuttleworth, 2000; Moneer and Taylor, 2002). It has been proposed that ARC is a major Ca^{2+} entry pathway required for oscillatory Ca^{2+} signaling (Shuttleworth, 1999; Mignen et al., 2001, 2003; see also Lankisch et al., 1999). In contrast, Luo et al. (2001) have suggested that an influx pathway distinct from both ARCs and SOCCs mediates Ca^{2+} entry that drives Ca^{2+} oscillations in HEK cells. The disparate conclusions of these studies underscore the need for extensive additional work to define the mechanisms of Ca^{2+} entry in nonexcitable cells, to define the role of SMOCCs and SOCCs in oscillatory Ca^{2+} signaling, and to identify molecular mechanisms of SMOCC and SOCC regulation.

As noted earlier, intracellular Ca^{2+} levels in the nematode intestine oscillate with a periodicity of 45–50 s (Dal Santo et al., 1999). These oscillations drive rhythmic contraction of body wall muscles and are dependent on IP_3 receptor function (Dal Santo et al., 1999). Both the ORCa and SOC channels could play central roles in generating and maintaining oscillatory Ca^{2+} signaling in the intestine. However, determination of their physiological functions requires in vitro and in vivo characterization of intestinal cell Ca^{2+} signaling events and identification of the genes that encode both channels. These studies are currently underway and will likely be facilitated by the genetic and molecular tractability of *C. elegans* as well as by the physiological accessibility of cultured intestinal cells.

Genetic and Molecular Analysis of the C. elegans Defecation Cycle

Mutagenesis and forward genetic analysis in *C. elegans* has to date identified ~12 genes that disrupt normal defecation rhythm when they are mutated (Iwasaki et al., 1995). *itr-1* and *flr-1*, which encodes a putative DEG/ENaC cation channel (Take-Uchi et al., 1998), are the only genes that have been mapped and characterized in detail. In addition, mutations in calcium/calmodulin-dependent serine/threonine kinase type II (CaMKII) have been shown to disrupt the defecation cycle (Reiner et al., 1999). CaMKII plays essential roles in oscillatory Ca^{2+} signaling (De Koninck and Schulman, 1998; Dupont and Goldbeter, 1998) and is expressed in multiple *C. elegans* cell types, including intestinal epithelial cells (unpublished observation cited in De Koninck and Schulman, 1998).

Mapping and characterization of mutant genes that disrupt defecation rhythm as well as isolation of other defecation mutants will likely provide unique insights into intestinal cell oscillatory Ca^{2+} signaling. It will also be important to utilize reverse genetic approaches to identify genes that encode the ORCa and SOC channels. At present, it is reasonable to postulate that the channels are encoded by one or more TRP genes (Montell, 2001; Clapham, 2002). The *C. elegans* genome contains 13 predicted TRP-encoding genes (3 TRPC, 5 TRPV, 4 TRPM, and 1 TRPN). Gene function in *C. elegans* can be rapidly and economically disrupted either by the use of chemical deletion mutagenesis or RNA interference (Barr, 2003; Strange, 2003). Deletion mutagenesis should allow definitive testing of the hypothesis that TRP genes encode the ORCa and SOC channels.

In conclusion, we have identified two highly Ca^{2+}-selective cation conductances in *C. elegans* intestinal epithelial cells. One conductance is store independent, and the other is activated by store depletion. Our studies provide the first detailed electrophysiological characterization of voltage-independent and store-operated Ca^{2+} conductances in *C. elegans*. The ability to combine patch clamp electrophysiological measurements on intestinal epithelial cells with forward and reverse genetic analyses provides a powerful new approach for defin-

ing the cellular and molecular mechanisms of IP_3-dependent oscillatory Ca^{2+} signaling and its role in controlling rhythmic biological processes.

We thank Drs. Joel Rothman and James McGhee for providing the *elt-2*–GFP-expressing worm strains JR1838 and JM63, respectively. We also thank Andrew M. Beld for technical assistance and Dr. Louis J. DeFelice for helpful discussions.

This work was supported by National Institutes of Health (NIH) grant DK51610. A.Y. Estevez was supported by a National Science Foundation postdoctoral fellowship. R.K. Roberts was supported by NIH Vanderbilt University Bridges Program grant GM60190-01S1.

Olaf S. Andersen served as editor.

Submitted: 21 January 2003
Accepted: 18 June 2003

REFERENCES

Almers, W., and E.W. McCleskey. 1984. Non-selective conductance in calcium channels of frog muscle: calcium selectivity in a single-file pore. *J. Physiol.* 353:585–608.

Aussel, C., R. Marhaba, C. Pelassy, and J.P. Breittmayer. 1996. Submicromolar La^{3+} concentrations block the calcium release-activated channel, and impair CD69 and CD25 expression in CD3- or thapsigargin-activated Jurkat cells. *Biochem. J.* 313:909–913.

Bakowski, D., and A.B. Parekh. 2002. Monovalent cation permeability and Ca^{2+} block of the store-operated Ca^{2+} current I_{CRAC} in rat basophilic leukemia cells. *Pflügers Arch.* 443:892–902.

Barr, M.M. 2003. Super models. *Physiol. Genomics.* 13:15–24.

Beedle, A.M., J. Hamid, and G.W. Zamponi. 2002. Inhibition of transiently expressed low- and high-voltage-activated calcium channels by trivalent metal cations. *J. Membr. Biol.* 187:225–238.

Berridge, M.J., P. Lipp, and M.D. Bootman. 2000. The versatility and universality of calcium signalling. *Nat. Rev. Mol. Cell Biol.* 1:11–21.

Bilmen, J., and F. Michelangeli. 2002. Inhibition of the type 1 inositol 1,4,5-trisphosphate receptor by 2-aminoethoxydiphenylborate. *Cell. Signal.* 14:955–960.

Bootman, M.D., P. Lipp, and M.J. Berridge. 2001. The organisation and functions of local Ca^{2+} signals. *J. Cell Sci.* 114:2213–2222.

Bootman, M.D., T.J. Collins, L. Mackenzie, H.L. Roderick, M.J. Berridge, and C.M. Peppiatt. 2002. 2-aminoethoxydiphenyl borate (2-APB) is a reliable blocker of store-operated Ca^{2+} entry but an inconsistent inhibitor of InsP3-induced Ca^{2+} release. *FASEB J.* 16: 1145–1150.

Brenner, S. 1974. The genetics of *Caenorhabditis elegans. Genetics.* 77: 71–94.

Christensen, M., A. Estevez, X. Yin, R. Fox, R. Morrison, M. McDonnell, C. Gleason, D.M. Miller, and K. Strange. 2002. A primary culture system for functional analysis of *C. elegans* neurons and muscle cells. *Neuron.* 33:503–514.

Christian, E.P., K.T. Spence, J.A. Togo, P.G. Dargis, and J. Patel. 1996. Calcium-dependent enhancement of depletion-activated calcium current in Jurkat T lymphocytes. *J. Membr. Biol.* 150:63–71.

Clapham, D.E. 2002. Sorting out MIC, TRP, and CRAC ion channels. *J. Gen. Physiol.* 120:217–220.

Clapham, D.E., L.W. Runnels, and C. Strubing. 2001. The TRP ion channel family. *Nat. Rev. Neurosci.* 2:387–396.

Dal Santo, P., M.A. Logan, A.D. Chisholm, and E.M. Jorgensen. 1999. The inositol trisphosphate receptor regulates a 50-second behavioral rhythm in *C. elegans. Cell.* 98:757–767.

De Koninck, P., and H. Schulman. 1998. Sensitivity of CaM kinase II to the frequency of Ca^{2+} oscillations. *Science.* 279:227–230.

Dolmetsch, R.E., and R.S. Lewis. 1994. Signaling between intracellular Ca^{2+} stores and depletion-activated Ca^{2+} channels generates $[Ca^{2+}]_i$ oscillations in T lymphocytes. *J. Gen. Physiol.* 103:365–388.

Dupont, G., and A. Goldbeter. 1998. CaM kinase II as frequency decoder of Ca^{2+} oscillations. *Bioessays.* 20:607–610.

Edgar, L.G. 1995. Blastomere culture and analysis. *Methods Cell Biol.* 48:303–321.

Elliott, A.C. 2001. Recent developments in non-excitable cell calcium entry. *Cell Calcium.* 30:73–93.

Fierro, L., and A.B. Parekh. 1999. Fast calcium-dependent inactivation of calcium release-activated calcium current (CRAC) in RBL-1 cells. *J. Membr. Biol.* 168:9–17.

Fierro, L., and A.B. Parekh. 2000. Substantial depletion of the intracellular Ca^{2+} stores is required for macroscopic activation of the Ca^{2+} release-activated Ca^{2+} current in rat basophilic leukaemia cells. *J. Physiol.* 522:247–257.

Fukushige, T., M.J. Hendzel, D.P. Bazett-Jones, and J.D. McGhee. 1999. Direct visualization of the elt-2 gut-specific GATA factor binding to a target promoter inside the living *Caenorhabditis elegans* embryo. *Proc. Natl. Acad. Sci. USA.* 96:11883–11888.

Goodman, M.B., D.H. Hall, L. Avery, and S.R. Lockery. 1998. Active currents regulate sensitivity and dynamic range in *C. elegans* neurons. *Neuron.* 20:763–772.

Gregory, R.B., and G.J. Barritt. 2003. Evidence that Ca^{2+}-release-activated Ca^{2+} channels in rat hepatocytes are required for the maintenance of hormone-induced Ca^{2+} oscillations. *Biochem. J.* 370:695–702.

Halaszovich, C.R., C. Zitt, E. Jungling, and A. Luckhoff. 2000. Inhibition of TRP3 channels by lanthanides. Block from the cytosolic side of the plasma membrane. *J. Biol. Chem.* 275:37423–37428.

Hermosura, M.C., M.K. Monteilh-Zoller, A.M. Scharenberg, R. Penner, and A. Fleig. 2002. Dissociation of the store-operated calcium current I_{CRAC} and the Mg-nucleotide-regulated metal ion current MagNuM. *J. Physiol.* 539:445–458.

Hille, B. 2001. Ion Channels of Excitable Membranes. 3rd ed. Sinauer Associates, Inc., Sunderland, MA. 814 pp.

Hoth, M. 1995. Calcium and barium permeation through calcium release-activated calcium (CRAC) channels. *Pflügers Arch.* 430: 315–322.

Hoth, M., and R. Penner. 1992. Depletion of intracellular calcium stores activates a calcium current in mast cells. *Nature.* 355:353–356.

Hoth, M., and R. Penner. 1993. Calcium release-activated calcium current in rat mast cells. *J. Physiol.* 465:359–386.

Iwasaki, K., and J.H. Thomas. 1997. Genetics in rhythm. *Trends Genet.* 13:111–115.

Iwasaki, K., D.W.C. Liu, and J.H. Thomas. 1995. Genes that control a temperature-compensated ultradian clock in *Caenorhabditis elegans. Proc. Natl. Acad. Sci. USA.* 92:10317–10321.

Kerschbaum, H.H., and M.D. Cahalan. 1998. Monovalent permeability, rectification, and ionic block of store-operated calcium channels in Jurkat T lymphocytes. *J. Gen. Physiol.* 111:521–537.

Kostich, M., A. Fire, and D.M. Fambrough. 2000. Identification and molecular-genetic characterization of a LAMP/CD68-like protein from *Caenorhabditis elegans. J. Cell Sci.* 113:2595–2606.

Kozak, J.A., H.H. Kerschbaum, and M.D. Cahalan. 2002. Distinct properties of CRAC and MIC channels in RBL cells. *J. Gen. Physiol.* 120:221–235.

Lankisch, T.O., F. Nozu, C. Owyang, and Y. Tsunoda. 1999. High-affinity cholecystokinin type A receptor/cytosolic phospholipase A2 pathways mediate Ca^{2+} oscillations via a positive feedback regulation by calmodulin kinase in pancreatic acini. *Eur. J. Cell Biol.* 78:632–641.

Lechleiter, J.D., and D.E. Clapham. 1992. Molecular mechanisms of intracellular calcium excitability in *X. laevis* oocytes. *Cell.* 69:283–294.

Lepple-Wienhues, A., and M.D. Cahalan. 1996. Conductance and permeation of monovalent cations through depletion-activated Ca^{2+} channels (I_{CRAC}) in Jurkat T cells. *Biophys. J.* 71:787–794.

Lewis, C.A. 1979. Ion-concentration dependence of the reversal potential and the single channel conductance of ion channels at the frog neuromuscular junction. *J. Physiol.* 286:417–445.

Lewis, J.A., and J.T. Fleming. 1995. Basic culture methods. *Methods Cell Biol.* 48:3–29.

Lewis, R.S. 2001. Calcium signaling mechanisms in T lymphocytes. *Annu. Rev. Immunol.* 19:497–521.

Luo, D., L.M. Broad, J. Bird, and J.W. Putney, Jr. 2001. Signaling pathways underlying muscarinic receptor-induced $[Ca^{2+}]_i$ oscillations in HEK293 cells. *J. Biol. Chem.* 276:5613–5621.

Mayer, M.L., G.L. Westbrook, and P.B. Guthrie. 1984. Voltage-dependent block by Mg^{2+} of NMDA responses in spinal cord neurones. *Nature.* 309:261–263.

Merritt, J.E., W.P. Armstrong, C.D. Benham, T.J. Hallam, R. Jacob, A. Jaxa-Chamiec, B.K. Leigh, S.A. McCarthy, K.E. Moores, and T.J. Rink. 1990. SK&F 96365, a novel inhibitor of receptor-mediated calcium entry. *Biochem. J.* 271:515–522.

Mignen, O., and T.J. Shuttleworth. 2000. I_{ARC}, a novel arachidonate-regulated, noncapacitative Ca^{2+} entry channel. *J. Biol. Chem.* 275: 9114–9119.

Mignen, O., J.L. Thompson, and T.J. Shuttleworth. 2001. Reciprocal regulation of capacitative and arachidonate-regulated noncapacitative Ca^{2+} entry pathways. *J. Biol. Chem.* 276:35676–35683.

Mignen, O., J.L. Thompson, and T.J. Shuttleworth. 2003. Ca^{2+} selectivity and fatty acid specificity of the noncapacitative, arachidonate-regulated Ca^{2+} (ARC) channels. *J. Biol. Chem.* 278:10174–10181.

Moneer, Z., and C.W. Taylor. 2002. Reciprocal regulation of capacitative and non-capacitative Ca^{2+} entry in A7r5 vascular smooth muscle cells: only the latter operates during receptor activation. *Biochem. J.* 362:13–21.

Montell, C. 2001. Physiology, phylogeny, and functions of the TRP superfamily of cation channels. *Sci. STKE.* 90:RE1–RE17.

Nadler, M.J., M.C. Hermosura, K. Inabe, A.L. Perraud, Q. Zhu, A.J. Stokes, T. Kurosaki, J.P. Kinet, R. Penner, A.M. Scharenberg, and A. Fleig. 2001. LTRPC7 is a Mg.ATP-regulated divalent cation channel required for cell viability. *Nature.* 411:590–595.

Nowak, L., P. Bregestovski, P. Ascher, A. Herbet, and A. Prochiantz. 1984. Magnesium gates glutamate-activated channels in mouse central neurones. *Nature.* 307:462–465.

Parekh, A.B. 1998. Slow feedback inhibition of calcium release-activated calcium current by calcium entry. *J. Biol. Chem.* 273:14925–14932.

Parekh, A.B., and R. Penner. 1997. Store depletion and calcium influx. *Physiol. Rev.* 77:901–930.

Petersen, O.H. 2002. Calcium signal compartmentalization. *Biol. Res.* 35:177–182.

Pizzo, P., A. Burgo, T. Pozzan, and C. Fasolato. 2001. Role of capacitative calcium entry on glutamate-induced calcium influx in type-I rat cortical astrocytes. *J. Neurochem.* 79:98–109.

Prakriya, M., and R.S. Lewis. 2001. Potentiation and inhibition of Ca^{2+} release-activated Ca^{2+} channels by 2-aminoethyldiphenyl borate (2-APB) occurs independently of IP_3 receptors. *J. Physiol.* 536:3–19.

Prakriya, M., and R.S. Lewis. 2002. Separation and characterization of currents through store-operated CRAC channels and Mg^{2+}-inhibited cation (MIC) channels. *J. Gen. Physiol.* 119:487–507.

Putney, J.W., Jr., and R.R. McKay. 1999. Capacitative calcium entry channels. *Bioessays.* 21:38–46.

Reiner, D.J., E.M. Newton, H. Tian, and J.H. Thomas. 1999. Diverse behavioural defects caused by mutations in *Caenorhabditis elegans* unc-43 CaM kinase II. *Nature.* 402:199–203.

Runnels, L.W., L. Yue, and D.E. Clapham. 2001. TRP-PLIK, a bifunctional protein with kinase and ion channel activities. *Science.* 291:1043–1047.

Shuttleworth, T.J. 1999. What drives calcium entry during $[Ca^{2+}]_i$ oscillations? - challenging the capacitative model. *Cell Calcium.* 25:237–246.

Strange, K. 2003. From genes to integrative physiology: Ion channel and transporter biology in *Caenorhabditis elegans*. *Physiol. Rev.* 83:377–415.

Take-Uchi, M., M. Kawakami, T. Ishihara, T. Amano, K. Kondo, and I. Katsura. 1998. An ion channel of the degenerin/epithelial sodium channel superfamily controls the defecation rhythm in *Caenorhabditis elegans*. *Proc. Natl. Acad. Sci. USA.* 95:11775–11780.

Taylor, C.W., and P. Thorn. 2001. Calcium signalling: IP_3 rises again, and again. *Curr. Biol.* 11:R352–R355.

Torihashi, S., T. Fujimoto, C. Trost, and S. Nakayama. 2002. Calcium oscillation linked to pacemaking of interstitial cells of Cajal. Requirement of calcium influx and localization of TRP4 in caveolae. *J. Biol. Chem.* 277:19191–19197.

Vennekens, R., J. Prenen, J.G. Hoenderop, R.J. Bindels, G. Droogmans, and B. Nilius. 2001. Pore properties and ionic block of the rabbit epithelial calcium channel expressed in HEK 293 cells. *J. Physiol.* 530:183–191.

Voets, T., J. Prenen, A. Fleig, R. Vennekens, H. Watanabe, J.G.J. Hoenderop, R.J.M. Bindels, G. Droogmans, R. Penner, and B. Nilius. 2001. CaT1 and the calcium release-activated calcium channel manifest distinct pore properties. *J. Biol. Chem.* 276:47767–47770.

Wu, X., G. Babnigg, T. Zagranichnaya, and M.L. Villereal. 2002. The role of endogenous human TRP4 in regulating carbachol-induced calcium oscillations in HEK-293 cells. *J. Biol. Chem.* 277: 13597–13608.

Zhang, L., and M.A. McCloskey. 1995. Immunoglobulin E receptor-activated calcium conductance in rat mast cells. *J. Physiol.* 483:59–66.

Zitt, C., C.R. Halaszovich, and A. Luckhoff. 2002. The TRP family of cation channels: probing and advancing the concepts on receptor-activated calcium entry. *Prog. Neurobiol.* 66:243–264.

Zweifach, A., and R.S. Lewis. 1993. Mitogen-regulated Ca^{2+} current of T lymphocytes is activated by depletion of intracellular Ca^{2+} stores. *Proc. Natl. Acad. Sci. USA.* 90:6295–6299.

Zweifach, A., and R.S. Lewis. 1995. Rapid inactivation of depletion-activated calcium current (I_{CRAC}) due to local calcium feedback. *J. Gen. Physiol.* 105:209–226.